Decorin is an early CSF biomarker of Alzheimer's Aβ amyloidosis

Richeng Jiang
Karolinska Institutet
Una Smailovic
Karolinska Institutet
Hazal Haytural
Karolinska Institutet
Robert Haret
Carol Davila University of Medicine and Pharmacy
Ganna Shevchenko
Uppsala University
Betty Tijms
Alzheimer Center Amsterdam, Department of Neurology, Amsterdam Neuroscience, Vrije Universiteit Amsterdam, Amsterdam UMC, the Netherlands https://orcid.org/0000-0002-2612-1797
Johan Gobom
University of Gothenburg, the Sahlgrenska Academy
Axel Abelein
Karolinska Institutet https://orcid.org/0000-0002-8079-3017
Nenad Bogdanovic
Karolinska Institutet
Henrik Zetterberg
University of Gothenburg https://orcid.org/0000-0003-3930-4354
bengt winblad
karolinska Instituet
Susanne Frykman
Division of Neurogeriatrics, Center for Alzheimer Research, Department of Neurobiology, Care Sciences and Society, Karolinska Institutet
Vesna Jelic
Karolinska Institutet
Jonas Bergquist
Uppsala University https://orcid.org/0000-0002-4597-041X
Pieter Jelle Visser
Amsterdam UMC
Per Nilsson (Per.et.Nilsson@ki.se)

Karolinska Institutet https://orcid.org/0000-0001-6450-0870

Article

Keywords: amyloid-beta (Aβ) amyloidosis, Alzheimer's disease (AD), CSF biomarkers

Posted Date: March 2nd, 2021

DOI: https://doi.org/10.21203/rs.3.rs-275229/v1

Version of Record: A version of this preprint was published at Alzheimer's & Dementia on December 1st, 2021. See the published version at https://doi.org/10.1002/alz.054474.

Abstract

Alzheimer's disease (AD) is characterized by impaired protein homeostasis leading to amyloid-beta (Aβ) amyloidosis. Here, we show that autophagy is similarly inhibited in AD brains and *App* knock-in AD mouse models. To determine how pathologies translate to cerebrospinal fluid (CSF), label-free mass spectrometry of mouse CSF was used. This identified autophagy-related extracellular matrix (ECM) protein decorin as significantly and similarly increased in *App* knock-in mice and cognitively normal human subjects with abnormal CSF-amyloid. Notably, a switch from negative to positive correlation of CSF-decorin and CSF-amyloid occurs in cognitively normal subjects when CSF-amyloid becomes abnormal, indicating an early change in CSF-decorin induced by Aβ amyloidosis. In *App* knock-in mice increased CSF-decorin correlated with accentuated decorin expression in choroid plexus and decreased interneuronal decorin. Furthermore, decorin activates neuronal autophagy-lysosomal system by enhancing lysosomal degradation. Therefore, decorin is a potential CSF biomarker that reflects ECM and autophagy alterations in early AD Aβ amyloidosis.

Introduction

Approximately 50 million people in the world are living with dementia and this number is estimated to triple by 2050 (*1*). Alzheimer's disease (AD) is the most common cause of dementia leading to cognitive impairment and decline. Since effective treatments are yet to be developed, more research on the pathogenesis of AD at the molecular level is warranted to understand and treat AD. Two pathological hallmarks are found in the AD brain parenchyma: extracellular amyloid-beta peptide (Aβ) depositions and intracellular tau aggregation. In addition, vascular changes such as cerebral atherosclerosis, large infarcts and microinfarcts and cerebral amyloid angiopathy (CAA) often accompany AD-associated neuropathology (*2*). CAA, observed in around 40% of AD cases, consists of vascular deposits of Aβ and can affect blood-brain-barrier (BBB) and blood-cerebrospinal fluid barrier (BCSFB) composition and potentially worsen disease progression (*2, 3*). Aβ also accumulats in the choroid plexus (ChP) in the AD brains causing ChP dysfunction (*4*) and tau pathology may additionally contribute to BBB dysfunction (*5*). The BBB is composed of endothelial cells in brain arteries and capillaries, basement membrane and pericytes, surrounded by astrocyte end-feet which together form the neuro-vascular unit (*6*). Because of the tight junction between the endothelial cells, BBB highly controls the molecular exchange between blood and brain parenchyma. However, disruption of BBB function including the tight junctions is frequently detected in AD brains. It may lead to imparied Aβ clearance from brain to the peripheral circulation which may aggrevate the Aβ accumulation in the brain that further increases BBB dysfuntion (*7*). During this vicious cycle, the basement membrane consisting of extracellular matrix (ECM) is affected. ECM is a highly dynamic network that consists of proteoglycans/glycosaminoglycans, collagen, elastin, fibronectin, laminins, and several other glycoproteins (*8*). Already during the early stages of AD, significant changes of ECM affect brain microvascular function and may therefore drive AD progression (*9*). However, whether the vascular changes are causes or consequnces of the brain pathologies remains to be fully elucidated.

App knock-in AD mouse models exhibit AD-like phenotypes including robust Aβ pathologies, but express APP at endogenous levels which circumvent potential drawbacks of APP overexpression associated with previous APP transgenic mice. Aβ is generated from cleavage of amyloid precursor protein (APP) by β- and γ- secretase. Insertion of two clinical mutations found in the *APP* gene in familial AD, the Swedish and the Beyreuther/Iberian mutations, to the mouse *App* gene leads to increased generation of Aβ42 in the $App^{NL\text{-}F/NL\text{-}F}$ line (*10*). In addition to the Swedish/Iberian mutations, the Arctic mutation was introduced in $App^{NL\text{-}G\text{-}F/NL\text{-}G\text{-}F}$ mice which has a more aggressive Aβ pathology starting at two months of age while the Aβ pathology of $App^{NL\text{-}F/NL\text{-}F}$ mice starts from nine months of age (*10*). This aggressive Aβ pathology of $App^{NL\text{-}G\text{-}F/NL\text{-}G\text{-}F}$ mice drives earlier and severer neuroinflammation, synaptic alteration and memory impairment as compared to $App^{NL\text{-}F/NL\text{-}F}$ mice (*10*).

In addition to the Aβ and tau pathologies, abnormal autophagy function has been observed in AD, characterized by autophagosome accumulation in dystrophic neurites of human and transgenic mouse AD brains (*11*). As one of the major intracellular clean-up systems, macroautophagy (herein referred to as autophagy) plays a crucial role in the metabolism of Aβ (*12*). Autophagy is initiated from the phagophore, a double membrane structure, which is induced by cargo receptors like sequestosome 1/p62 and NBR1 (*13*). In the p62 dependent autophagy pathway, p62 binds to microtubule-associated protein 1 light chain 3 (LC3) and participates in autophagosome formation. P62 delivers targets to be degraded by autophagy and is eventually degraded by the lysosome (*14*). During phagophore elongation, autophagy-related gene (Atg) 5 is conjugated with Atg12 which interacts with Atg16L to form Atg5-Atg12-Atg16L complexes and these complexes are indispensable in autophagosome formation (*15*). In addition, ubiquitin-like protein Atg8/LC3 is also involved in autophagosome formation by covalently conjugated to phosphatidylethanolamine (*16*). LC3 I, which is generated from LC3 cleaved by cysteine protease Atg4B, is conjugated with PE to form LC3 II (*17, 18*). LC3 II is therefore a specific autophagosome associated marker (*19*) and both p62 and LC3II are commonly used for measuring autophagy flux (*20*). Subsequently, the completed autophagosomes fuse with lysosomes to form autolysosomes, which degrade the autophagic contents. In AD brains, an accumulation of autophagosomes accompanied by increased levels of lysosomal proteases is observed (*21*). This together with gene expression analysis showing an increase in the expression of autophagy-related genes indicate that autophagy is activated in the early stage whereas it becomes impaired in the late stage of the disease (*22-25*).

Investigation of the two body fluids, plasma and cerebrospinal fluid (CSF) may give insights into AD brain pathology and biomarker discovery (*26*). Indeed, a growing number of clinical research data support that the biomarkers of CSF play an important role in AD diagnostics (*27*). CSF is mainly produced by the ChP of the ventricles and has close physical interaction with the brain, whereafter it is drained through the dural venous sinuses and the lymphatic system, indicating that the proteins in CSF may directly reflect the brain pathology (*26*). Three core CSF biomarkers, Aβ42, total-tau (t-tau) and phosphorylated-tau (p-tau), are used in the clinic to diagnose AD patients (*28*). However, to be able to distinguish AD from other forms of dementia such as Lewy body dementia, frontotemporal dementia and vascular dementia, as

well as to predict AD progression, further investigations are needed for understanding the biological complexity of AD and how it translates to CSF (*29*).

The aims of this study are: firstly, to characterize the autophagy status in *App* knock-in mice and compare it with AD postmortem brains; secondly, to search for protein alterations that are mirrored in CSF of *App* knock-in mice by label-free mass spectrometry (MS) and, thirdly, to identify proteins which are similarly changed in CSF of human subjects across the AD spectrum. Here, we identified the autophagy-related ECM protein decorin as similarly and significantly altered in CSF of both $App^{NL\text{-}F/NL\text{-}F}$ mice and preclinical AD subjects having abnormal-amyloid/normal-tau (a+t-). In addition, we found that decorin stimulates the neuronal autophagy-lysosomal pathway by enhancing lysosomal degradation.

Results

Autophagy is impaired in AD brains

p62 is a cargo receptor that recognizes and transports ubiquitinated proteins to autophagosomes to be degraded by lysosomes. p62 is normally degraded along with the cargo during functional autophagy and therefore, p62 accumulation and aggregation indicate impaired autophagy. To investigate autophagy status in AD brains, we immunostained brains from healthy controls (**Fig. 1a-e**) and AD subjects (**Fig. 1f-j**) for p62 and quantified the p62-positive signals. The results showed a pronounced p62 accumulation in both cortex (**Fig. 1f**) and hippocampus including dentate gyrus (DG) (**Fig. 1g**), CA1 (**Fig. 1h**), and CA3 (**Fig. 1i**) of AD brains (semi-quantified in **Fig 1k,l**), whereas no p62 accumulation was found in brains of non-demented individuals (**Fig. 1a-d**). p62 accumulated as large intracellular aggregations in neurons (**Fig. 1f and 1g,** arrow in depicted area 1**, Fig. 1h,** arrow in depicted area) and was also identified as small round dots or outstretched structures (**Fig. 1f and 1g,** arrows in depicted area 2). This dot-shaped staining may represent axonal beadings, which are the series of swellings along the axons located in the molecular layer of DG. In addition, we found p62 in apoptotic bodies (**Fig. 1i,** arrows in depicted area) and corpora amylacea (**Fig. 1j,** arrows in depicted area). Interestingly, tunica intima of the vessels also contains substantial amount of p62-postive staining (**Fig. 1j**). In summary, p62 accumulation was frequently observed in AD brains, which indicates a disturbed autophagy-lysosomal system potentially caused by an inhibition of autophagy in both neurons and cells in the tunica intima of vessels.

To further characterize alterations in the autophagy system in AD brains, we analyzed another autophagy key protein in the autophagy pathway, Atg5, in AD postmortem brains. The results showed that Atg5 was significantly upregulated in neurons in cortex (**Extended Data Fig. 1f**) and in the hippocampus (granular cell layer of DG (**Extended Data Fig. 1g**), CA1 (**Extended Data Fig. 1h**), and CA3 (**Extended Data Fig. 1i**)) of AD brains as compared to healthy control brains (**Extended Data Fig. 1a-e**) (semi-quantified in **Extended Data Fig 1k,l**). Interestingly, we found that Atg5 was not only increased in the neurons (**Extended Data Fig. 1f,g,h,i,** arrows in depicted area) but also in glial cells (**Extended Data Fig. 1j,** arrow in depicted area), potentially as an attempt to increase autophagy in those cells.

Autophagy is impaired in *App*$^{NL-G-F/NL-G-F}$ mice

We next asked the question if autophagy is altered in two *App* knock-in AD mouse models, *App*$^{NL-F/NL-F}$ and *App*$^{NL-G-F/NL-G-F}$ mice. The two models exhibit different degree of Aβ pathology, neuroinflammation, synaptic alteration and cognitive impairment all of which being significantly stronger in the *App*$^{NL-G-F/NL-G-F}$ mice due to the arctic mutation which enhances Aβ oligomerization (*10*) (**Fig. 2a,b**). To characterize the autophagy status in the *App* knock-in mice, we performed western blot and immunohistochemical analysis for autophagy markers LC3 and p62 using 12 months old homozygous *App*$^{wt/wt}$, *App*$^{NL-F/NL-F}$ and *App*$^{NL-G-F/NL-G-F}$ mouse brains. We found that both p62 and LC3 II were specifically increased in the cortex of *App*$^{NL-G-F/NL-G-F}$ mice but not in *App*$^{NL-F/NL-F}$ mice as compared with *App*$^{wt/wt}$ mice (**Fig. 2c,d**). In addition, the LC3 II levels were also significantly increased in the hippocampus of *App*$^{NL-G-F/NL-G-F}$ mice whereas it was decreased in the *App*$^{NL-F/NL-F}$ mice as compared to *App*$^{wt/wt}$ mice (**Fig. 2e,f**). Consistently, immunostaining of p62 showed a significant accumulation of p62 in *App*$^{NL-G-F/NL-G-F}$ mice as compared to *App*$^{wt/wt}$ (**Fig. 2g,h**), whereas the p62 mRNA expression level was unaltered (**Fig. 2i**). These data together show that autophagy is inhibited in the brains of *App*$^{NL-G-F/NL-G-F}$ mice.

ECM and autophagy related proteins are altered in CSF of *App* knock-in mice

In a translational approach to identify potential AD-related biomarkers including alterations in proteins associated with or regulating autophagy, we next investigated CSF of the 12 months old *App*$^{NL-F/NL-F}$, *App*$^{NL-G-F/NL-G-F}$, and *App*$^{wt/wt}$ mice. Taking the limited volume of mouse CSF into account, a label-free MS approach was used for the detection and quantification of the mouse CSF proteomes. This led to the identification of 427-703 proteins (a complete list of all identified proteins is presented in **Supplementary Table 1**). A qualitative analysis of proteins that were detected in all 12 samples, revealed that 246 proteins were identified in all three groups while some proteins were identified only in two of the groups and some proteins were uniquely detected in one group (**Fig. 3a**). Principal component analysis (PCA) of the CSF proteome using the 246 proteins identified in all the samples indicated a separation between the three groups (**Fig. 3b**). Among the proteins that were significantly changed ($p < 0.05$) in *App*$^{NL-F/NL-F}$ and *App*$^{NL-G-F/NL-G-F}$ mice as compared to *App*$^{wt/wt}$ mice, 13 proteins were commonly changed whereas 25 and 23 proteins were specifically changed in either *App*$^{NL-F/NL-F}$ or *App*$^{NL-G-F/NL-G-F}$ mice respectively (**Fig. 3c**). PCA of the significantly altered proteins ($p < 0.05$) resulted in a tighter clustering of the three groups (**Fig. 3d**). Volcano plots visualized a similar number of up and downregulated proteins in both *App*$^{NL-F/NL-F}$ and *App*$^{NL-G-F/NL-G-F}$ mouse CSF as compared to *App*$^{wt/wt}$ mice (**Fig. 3e,f**, protein list in **Supplementary Table 2**). A detailed list of significantly ($p < 0.05$) altered proteins are shown in the heatmap (**Fig. 3g,h**). Among those significantly altered proteins, two proteins (Cathepsin B and Alpha-mannosidase) are associated with autophagy and seven proteins (SPARC-like protein 1, fibronectin, ecm1 protein, collagen alpha-1(I), basement membrane-specific heparan sulfate proteoglycan core protein, fibulin-1, vitronectin) are ECM proteins (**Table 1**). Interestingly, two proteins, decorin and lumican, are related to both autophagy and ECM and significantly increased in *App*$^{NL-F/NL-F}$ mice as compared to *App*$^{wt/wt}$ (**Table 1**). Comparing the

two *App* knock-in mouse models directly with each other revealed significant ($p < 0.05$) changes in additional autophagy and ECM related proteins (**Extended Data Fig. 2a,b, Table 1**). Taking these data together indicate that $App^{NL\text{-}F/NL\text{-}F}$ and $App^{NL\text{-}G\text{-}F/NL\text{-}G\text{-}F}$ mice are, at least to some extent, different mouse models of AD, which may also include the autophagy status reflected in their CSF proteomes.

Several studies have previously found that the dysfunction of BBB and BCSFB, including changes in ECM proteins, increase upon aging and in AD (*30-32*). Therefore, to identify additional brain barrier changes in the CSF from the *App* knock-in mice not detected by the MS analysis, we also analyzed the CSF of 18 months old *App* knock-in mice (n = 5) using a mouse proximity extension assay **(**PEA) panel containing several autophagy and ECM associated proteins (but not including decorin and lumican). From a panel of 92 proteins, one autophagy associated protein (Tripeptidyl-peptidase 1) and two ECM associated proteins (Matrilin-2 and CCN family member 4) were significantly ($p < 0.05$) altered in *App* knock-in mice (**Table 1, Supplementary Table 3**). In addition, indispensable BBB associated protein platelet-derived growth factor subunit B, was significantly decreased in $App^{NL\text{-}G\text{-}F/NL\text{-}G\text{-}F}$ mice as compared to $App^{NL\text{-}F/NL\text{-}F}$ mice (**Supplementary Table 3**). Altogether, the analysis of CSF from *App* knock-in mice by MS and PEA showed alterations in both autophagy and ECM-related proteins as well as BBB-associated proteins indicating changes in the BBB/BCFCB. Interestingly, decorin and lumican which are related to both autophagy and ECM are significantly altered in the CSF of $App^{NL\text{-}F/NL\text{-}F}$ mice but not in that of $App^{NL\text{-}G\text{-}F/NL\text{-}G\text{-}F}$ mice which indicates that changes in the CSF of these two proteins could reflect the early events in the development of the pathologies in the *App* knock-in mice.

Decorin is similarly increased in CSF of $App^{NL\text{-}F/NL\text{-}F}$ mice and in CSF of preclinical AD subjects having abnormal amyloid

In an attempt to further understand how changes in the mouse CSF proteomes of the AD mouse models reflect those observed in patients, we next compared them to MS-characterized CSF proteomes of a large human cohort European Medical Information Framework for Alzheimer's Disease Multimodal Biomarker Discovery (EMIF-AD MBD) (*33*). According to the specific criteria, individuals with abnormal CSF Aβ42 were classified into three clinical stages; preclinical AD (normal cognition, *i.e.*, NC), prodromal AD (mild cognitive impairment, *i.e.*, MCI) and mild to moderate AD-type dementia, based on their cognitive performance (*34*). The CSF proteome alterations in NC, MCI and AD were based on the comparison to the control subjects having normal CSF Aβ42 and tau, and normal cognition.

Since the present study is an exploratory study, we chose to perform two kinds of comparisons of the mouse and human proteomes. Firstly, we compared how many proteins with relative expression levels below one and above one as compared to healthy controls, were common in the mouse and human CSF proteomes. Secondly, we analyzed the number of proteins with significantly changed expression levels that were commonly altered in both mouse and human CSF proteomes. Because of *App* knock-in mice exhibit robust Aβ pathology but less pronounced tau pathology ($App^{NL\text{-}G\text{-}F/NL\text{-}G\text{-}F}$ mice have higher tau phosphorylation at Ser-396/Ser-404, and Ser-422 as compared to $App^{wt/wt}$ mice, but lack neurofibrillary tangles) (*35*), their CSF proteomes were compared with human proteomes stratified for CSF t-tau status

i.e., abnormal-amyloid/abnormal-tau (a+t+) (**Supplementary Table 4**) and abnormal-amyloid/normal-tau (a+t-) (**Supplementary Table 5**). Though a similar number of commonly upregulated proteins comparing the mouse and human cohorts was found, the comparison revealed that 76-90 proteins were commonly downregulated in mouse and a+t- human subjects whereas much fewer, 24-29 proteins, were commonly downregulated in mouse and a+t+ human subjects (**Fig. 4a**). This indicated that alterations in CSF proteome of *App* knock-in mice are, at least to some extent, more similar to the CSF alterations observed in a+t- human subjects which may reflect that *App* knock-in mice have a strong Aβ pathology whereas the tau pathology is less pronounced. Further analyses were therefore performed in a+t- human subjects.

A qualitative direct comparison of CSF MS data from patients and $App^{NL\text{-}F/NL\text{-}F}$ mice, as presented in the Venn diagrams, showed that 33, 46 and 35 proteins exhibited a relative expression level above one whereas 76, 84 and 81 proteins were below one in NC, MCI and AD, respectively, and $App^{NL\text{-}F/NL\text{-}F}$ mice (**Fig. 4b**, protein list in **Supplementary Table 5**). Notably, restricting the comparisons to the proteins with significantly altered levels ($p < 0.05$), only one protein decorin (*DCN*), was found to be significantly upregulated in both NC subjects and $App^{NL\text{-}F/NL\text{-}F}$ mice (**Fig. 4c**). In the MCI vs $App^{NL\text{-}F/NL\text{-}F}$ mouse comparison six proteins, including one ECM protein, SPARC-like protein 1 (*SPARCL1*), as well as two BBB-associated proteins, dickkopf-3 (*DKK3*) and neurotrimin (*NTM*), were significantly and commonly downregulated. In the AD vs $App^{NL\text{-}F/NL\text{-}F}$ mouse comparison the same proteins that were altered in the MCI vs $App^{NL\text{-}F/NL\text{-}F}$ mouse comparison were found to be altered. In addition, one ECM protein, fibronectin (*FN1*), and one BBB-associated protein, contactin-1 (*CNTN1*), were commonly and significantly altered in the AD vs $App^{NL\text{-}F/NL\text{-}F}$ mouse comparison (**Fig. 4d**). Comparing $App^{NL\text{-}G\text{-}F/NL\text{-}G\text{-}F}$ mouse CSF proteome with the human CSF proteome revealed that 38, 50 and 37 proteins exhibited expression levels above one whereas 84, 90 and 86 proteins exhibited expression levels below one in NC, MCI, AD, respectively (**Fig. 4e**, protein list in **Supplementary Table 5**). Restricting the comparisons to only the significantly ($p < 0.05$) changed proteins (**Fig. 4f**), apolipoprotein A1 *(APOA1*) and apolipoprotein A2 (*APOA2*) which are related to cognitive status and late-onset AD (*36, 37*), were significantly upregulated in both AD subjects and $App^{NL\text{-}G\text{-}F/NL\text{-}G\text{-}F}$ mice whereas nine proteins including two ECM proteins, SPARC-like protein 1 (*SPARCL1*) and ecm1 protein (*ECM1*), and two BBB-associated proteins, limbic system–associated membrane protein (*LSAMP*) and natriuretic peptide precursor C (*NPPC*), were significantly and commonly downregulated in MCI. In AD, one additional ECM protein fibronectin (*FN1*) was similarly and significantly altered, as well as one additional BBB-associated proteins contactin-1 (*CNTN1*) was significantly and commonly downregulated (**Fig. 4g**). Taken together, the comparison of mouse and human CSF proteomes revealed that several ECM and BBB/BCSFB-associated proteins were significantly and commonly altered, indicating that the *App* knock-in mice recapitulate to some extent the changes observed in human CSF. Among the ECM proteins, decorin was found to be the earliest altered protein as shown by a significant increase in both $App^{NL\text{-}F/NL\text{-}F}$ mice having a mild and limited Aβ pathology, and preclinical a+t- subjects, whereas the cohorts representing the later stages in the AD spectrum *i.e.* MCI and AD did not exhibit a significant increase of decorin.

The correlation of CSF-decorin with CSF-amyloid switches from negative to positive upon onset of abnormal CSF-amyloid

We next studied in human CSF how decorin levels were related to the CSF AD biomarkers Aβ amyloid, t-tau and p-tau. Within the NC group, CSF-decorin levels follow a non-linear trajectory, with higher levels of decorin corresponding to lower CSF-amyloid in a-t- subjects, albeit not significantly (beta(se) = -0.16(0.18), p = 0.36) (**Fig. 5a**). In contrast, lower CSF-decorin levels corresponded to lower CSF-amyloid levels in a+t- subjects (beta(se) = 0.61(0.25), p = 0.01), a correlation that is significantly (p = 0.016) different from that of a-t- subjects (**Fig. 5a**). In other words, in subjects with pathological levels of CSF-amyloid, CSF-decorin levels tend to increase with decreased CSF-amyloid levels towards reaching abnormal CSF-amyloid. When CSF-amyloid levels are abnormal, the correlation switches and becomes positive. In addition, plotting CSF-decorin against CSF-t-tau and CSF-p-tau within the NC group reveals non-linear associations between decorin and t-tau or p-tau in a-t- subjects, whereas the correlations become significantly negative in a+t- subjects for both decorin and t-tau (beta(se) = -0.89(0.32), p = 0.0053) (**Fig. 5b**) and decorin and p-tau (beta(se) = -1.00(0.21), p < 0.0001) (**Fig. 5c**). Furthermore, across the total group including NC, MCI and AD subjects (n=310), lower CSF-decorin levels were related to higher CSF-t-tau (beta(se) = -0.11(0.04), p = 0.0014) (**Fig. 5e**) and CSF-p-tau levels (beta(se) = -0.16(0.04), p < 0.0001) (**Fig. 5f**), but no association with CSF-amyloid levels was observed (beta(se) = 0.09(0.06); p = 0.11) (**Fig. 5d**). Taken together, a switch from negative to positive correlation of CSF-decorin and CSF-amyloid occurs in NC a+t- subjects when CSF-amyloid reaches pathological levels, and at this stage, decorin additionally negatively correlates with both CSF-t-tau and CSF-p-tau. In addition, CSF-decorin levels continuously decreases with higher CSF-t-tau and CSF-p-tau levels in the whole AD spectrum. This indicates early change in CSF-decorin is associated with Aβ amyloidosis.

ECM associated biological processes were similarly changed both in *App* knock-in mouse models and human subjects with a+t-

Considering that a similar number of proteins exhibit levels either below one or above one in both $App^{NL-F/NL-F}$ and $App^{NL-G-F/NL-G-F}$ mice as compared to the a+t- human subjects (**Fig. 4a**), we decided to investigate whether those proteins are the same. This comparison also allowed us to detect changes that occur throughout the course of AD both in human and mouse as well as to pinpoint the ones that were specifically altered in one of the *App* knock-in mouse models. The Venn diagrams show that nine to 18 proteins were exclusively changed in one of the *App* knock-in mouse models and similarly changed in NC, MCI and AD human subjects, indicating that unique proteins are changed in the two *App* knock-in mouse models (**Extended Data Fig. 3a**). To get a better understanding of which biological processes are enriched from those exclusively changed proteins, we performed gene ontology enrichment analyses (protein list used for gene ontology is in **Supplementary Table 6**). Interestingly, the enrichment analyses revealed several pathways related to the ECM; collagen fibril organization, collagen catabolic process, extracellular matrix organization and extracellular matrix disassembly, as well as one pathway related to glycosaminoglycan metabolism; mucopolysaccharide metabolic process (**Extended Data Fig. 3b,c**). This

data indicated that changes in BBB/BCSFB composition may be present in the *App* knock-in mice which similarly takes place in human subjects with a+t- in the CSF.

Decorin is increased in the ChP of $App^{NL-F/NL-F}$ mice and decreased in parvalbumin (PV) positive interneuron neurites of $App^{NL-G-F/NL-G-F}$ mice

Having found that decorin was increased in CSF of $App^{NL-F/NL-F}$ mice, we were interested in the potential decorin alterations in the mouse brains since the pathological changes in the brain can translate to CSF. Therefore, we investigated the brains of the 12 months old mice used for CSF collection and performed immunohistochemistry of decorin to characterize decorin expression and localization. Interestingly, by establishing an immunostaining protocol based on the removal of glycosaminoglycan sidechains, we were able to successfully localize decorin in ChP, blood vessels and neurons. Indeed, decorin expression was significantly higher in ChP in $App^{NL-F/NL-F}$ mice as compared to $App^{wt/wt}$ mice but unaltered in $App^{NL-G-F/NL-G-F}$ mice (**Fig. 6a,b**). In addition to that, we found that decorin was highly expressed in the tunica externa of arteries (**Extended Data Fig. 4a**) and veins (**Extended Data Fig. 4b**) on the surface of the brain but not present in the vessels of brain parenchyma (**Extended Data Fig. 4c**). However no significant differences in decorin levels were observed in the vessels (**Extended Data Fig. 4d,e**).

Examining the brain parenchyma, we found that decorin was localized in neurons in both hippocampus and cortex. In hippocampus, decorin was not only expressed in CA2 pyramidal neurons but also in some other neurons of CA layers. To identify the decorin-positive neuronal subtype we performed double staining of decorin with two interneuronal markers, PV and somatotropin release-inhibiting factor (SRIF) (*38*). The results showed that a majority of decorin positive neurons co-localized with PV positive interneurons (**Fig. 6c**) whereas there was only a minor co-localization with SRIF positive interneurons (**Fig. 6d**). The quantification showed that the distributions of decorin positive cells in $App^{wt/wt}$, $App^{NL-F/NL-F}$, and $App^{NL-G-F/NL-G-F}$ mice were: more than 50% of decorin was found in CA2 pyramidal neurons, PV positive interneurons account for 30-40%, whereas approximately 10% were SRIF positive interneurons or other cell types (**Extended Data Fig. 5**). Although the distribution of decorin expressing cells were not different between *App* knock-in and $App^{wt/wt}$ mice, the decorin positive interneuron neurites of *App* knock-in mice, especially in the $App^{NL-G-F/NL-G-F}$ mice, contained significantly less decorin (**Fig. 6e,f**) as compared to $App^{wt/wt}$ mice.

Decorin levels in CSF correlates with Aβ pathology in the brains of $App^{NL-F/NL-F}$ mice

To better understand how Aβ amyloidosis is associated with both autophagy status and decorin expression in *App* knock-in mice as well as how these changes can be mirrored in the CSF, we performed Spearman's correlation analysis of Aβ plaque load, p62 and LC3 II levels, decorin expression in the brains and CSF-decorin levels. The analysis of the data from $App^{wt/wt}$ and $App^{NL-F/NL-F}$ mice (**Fig. 7a**) showed that the CSF-decorin levels positively correlated with both decorin expression in ChP ($r = 0.79$, $p = 0.028$) and Aβ plaque load in cortex ($r = 0.76$, $p = 0.04$). In addition, the LC3 II levels in hippocampus negatively correlated with Aβ plaque load in hippocampus ($r = -0.84$, $p = 0.017$), CSF-decorin levels ($r = -0.86$, $p =$

0.011) and decorin expression in Chp (r = -0.93, p = 0.002). Moreover, the decorin expression in the ChP negatively correlated with decorin in interneuron neurites (r = -0.74, p = 0.046). All these together indicated that autophagy is altered during early Aβ amyloidosis and the increase of CSF-decorin correlates with the increase of decorin in ChP possibly driven by the mild Aβ pathology in *App*$^{NL-F/NL-F}$ mice.

The correlation analysis of the data obtained from *App*$^{wt/wt}$ and *App*$^{NL-G-F/NL-G-F}$ mice (**Fig. 7b**) showed that both p62 (r = 0.86, p = 0.012) and LC3 II (r = 0.89, p = 0.006) positively correlated with Aβ plaque load in cortex whereas only LC3 II positively correlated with Aβ plaque load in hippocampus (r = 0.77, p = 0.033). The decorin expression in interneuron neurites negatively correlated with Aβ plaque load (r = -0.91, p = 0.005) and LC3 II (r = -0.93, p = 0.002) in hippocampus. In sharp contrast to the *App*$^{wt/wt}$ and *App*$^{NL-F/NL-F}$ dataset, the CSF-decorin levels in *App*$^{wt/wt}$ and *App*$^{NL-G-F/NL-G-F}$ dataset did not correlate with any of the measured parameters. The correlation findings indicate that the autophagy impairment and the reduced decorin expression in the interneurons were caused by the severe Aβ amyloidosis in *App*$^{NL-G-F/NL-G-F}$ mice whereas the correlation of decorin levels in CSF and in Chp with Aβ is lost in the *App*$^{NL-G-F/NL-G-F}$ mice.

Decorin activates autophagy-related lysosomal degradation in primary neurons

Having found that autophagy was inhibited in *App*$^{NL-G-F/NL-G-F}$ mouse brains and that less decorin was expressed in the neurites of hippocampal interneurons in *App*$^{NL-G-F/NL-G-F}$ mice together with the previous findings that decorin activates autophagy in endothelial cells (*39*) prompted us to investigate the relationship between decorin and autophagy in a neuronal setting. We, therefore, treated primary cortical/hippocampal neuron culture derived from *App*$^{wt/wt}$ mice with decorin and measured the effect of decorin on autophagy flux as determined by p62 and LC3 western blot analysis. The single decorin treatment data showed that decorin significantly decreased LC3 II and LC3 II/LC3 I ratio as compared to control and also a tendency towards decreased p62 level (p = 0.0891) (**Fig. 8a,b**). Furthermore, co-treatment with bafilomycin A1 (an inhibitor of lysosomal proteolysis) and decorin led to no change of LC3 II and p62 levels but an increase of LC3 II/LC3 I level as compared to Bafilomycin A1 treatment alone (**Fig. 8c,d**). However, the reason for the increase of LC3 II/LC3 I was from LC3 I reduction (**Fig. 8d**). All these together indicated that decorin activates autophagy-associated lysosomal degradation rather than causing an upstream induction of autophagy in *App*$^{wt/wt}$ primary neurons.

Discussion

Autophagy is altered in most neurodegenerative diseases, which share the common feature of dysfunctional protein homeostasis leading to aberrant protein aggregation (*40*). Although the genetic evidence for the involvement of autophagy in neurodegenerative diseases is strongest for Parkinson's disease and a genetic link between autophagy in AD is still to be found, the biochemical evidence for a dysfunctional autophagy-lysosomal system in AD is compelling (*40-42*). An accumulation of autophagosomes paralleled with increased levels of lysosomal proteases in brain tissues indicate that

the autophagic activity is upregulated early in the disease while it at later stages seems to collapse (*21-25*). Here we further substantiate these findings by showing that p62, which is normally metabolized by autophagy, accumulates in the neurons, vessels, corpora amylacea, potential axonal beadings and apoptotic bodies of AD brains, showing that autophagy is impaired in AD brains. Simultaneously, we also found an increase of Atg5 in neurons but also glial cells, indicative of potential attempts to upregulate autophagy possibly as a response to the increasing pathologies in the AD brain. To further investigate the relationship between Aβ amyloidosis and autophagy, taking into account that autophagy plays a key role in Aβ metabolism (*43*), we analyzed the brains of *App* knock-in mice, which recapitulate the Aβ pathology and the accompanied neuroinflammation and synaptic loss observed in AD without overexpression of APP. Interestingly, we observed, similar to AD brains, an inhibition of autophagy in the $App^{NL\text{-}G\text{-}F/NL\text{-}G\text{-}F}$ mice whereas the autophagy system was less affected in the $App^{NL\text{-}F/NL\text{-}F}$ mice as determined from p62 and LC3 analysis. This shows that the extent of Aβ pathology directly, or its downstream effects, will determine the effects on autophagy; the more severe Aβ pathology induced by the arctic mutation affects autophagy more than the less severe Aβ pathology present in the $App^{NL\text{-}F/NL\text{-}F}$ mice. Indeed, a strong correlation between Aβ pathology and the autophagy status was found both in cortex and hippocampus especially in $App^{NL\text{-}G\text{-}F/NL\text{-}G\text{-}F}$ mice. Moreover, the impaired autophagy may also induce aggregation of intracellular Aβ and potentially cause a vicious cycle. However, further cell-type specific analysis will undoubtedly shed more light into the detailed effects of the different Aβ pathologies, and their downstream events, on the different cell types in the brain including neurons, microglia and astrocytes.

To further understand the pathology including autophagy dysfunction in the brains of the *App* knock-in mouse models, how it is mirrored in the CSF and its translational potential toward clinical use, a MS analysis of the mouse CSF was performed. The analysis of the mouse CSF proteomes revealed alterations in several autophagy related proteins, including decorin and lumican, which are constituents of the ECM of BBB/BCSFB. Interestingly, decorin and lumican are highly expressed in the recently identified vascular cell type fibroblast-like cells which reside within the perivascular Virchow–Robin space in the mouse brain (*44*). The perivascular pathway facilitates CSF flow and enhances the clearance of Aβ (*45*). Of most importance in our study, decorin was similarly and significantly increased in CSF from both $App^{NL\text{-}F/NL\text{-}F}$ mice and NC a+t- human subjects. In addition, among NC subjects, a significant switch from negative to positive correlation of CSF-decorin and CSF-amyloid were found in the a+t- subjects as compared to a-t-subjects. That is, less CSF-decorin corresponds to less CSF-amyloid. Lowered CSF-amyloid is a key event in the onset and diagnosis of AD. Similarly, the CSF-decorin levels correlated with both CSF-t-tau and CSF-p-tau, both diagnostic criteria for AD, in a+t- subjects and the associations of CSF-decorin and CSF-t-tau or CSF-p-tau were continuously negative during the whole AD spectrum. Taken these together indicates that CSF-decorin changes are driven by early Aβ amyloidosis and that the CSF-decorin levels continue to decrease upon disease progression characterized by lower CSF-amyloid and higher CSF-tau. Other ECM proteins that were similarly changed in the $App^{NL\text{-}F/NL\text{-}F}$ mice and human subjects across the AD spectrum included SPARC-like protein 1 and fibronectin. In addition to these proteins, ecm1 protein was also altered in the CSF of $App^{NL\text{-}G\text{-}F/NLG\text{–}F}$ mice which exhibit a more severe pathology indicating that the ECM composition continues to alter during the later stage of the

development of the pathology in the brain. The fact that these proteins were found to be significantly altered and following the same direction of change between *App* knock-in mouse models and human cohorts emphasize that such changes are indeed translational between mice and human, and therefore, could hold a potential of serving as novel CSF biomarkers of ECM alterations. Indeed, the pathway analysis on the specific alterations in the two *App* knock-in models *versus* human CSF proteomes identified several biological pathways related to ECM processes including extracellular matrix organization, collagen fibril organization and mucopolysaccharide metabolism which were only enriched in the $App^{NL\text{-}F/NL\text{-}F}$ mice whereas extracellular matrix disassembly was enriched in the $App^{NL\text{-}G\text{-}F/NL\text{-}G\text{-}F}$ mice. Considering that the BBB is most likely affected in AD as several studies have indicated a breakdown of BBB (*46*), our proteomic findings suggest that the *App* knock-in mice could also have changes in the BBB/BCSFB. Although a dysfunctional BBB/BCSFB remains to be established in the *App* knock-in mice and the underlying causes of such a change remain to be elucidated, one possible reason could be the presence of CAA.

Decorin, as an ECM proteoglycan protein, has been previously identified in Aβ depositions in AD brains (*47*) whearas a disturbed decorin expression is observed in fibroblasts from sporadic AD patients (*48*). Using immunohistochemistry, we additionally show that decorin is highly expressed in CA2 pyramidal neurons and PV positive interneurons in hippocampus. Interestingly, the decorin expression in PV positive interneurons is decreased in *App* knock-in mice especially in $App^{NL\text{-}G\text{-}F/NL\text{-}G\text{-}F}$ mice. Furthermore, we also showed that decorin expression in ChP is increased in $App^{NL\text{-}F/NL\text{-}F}$ mice which correlates both with Aβ pathology and elevated CSF decorin level. Taken these data together indicates that early Aβ amyloidosis in the brain may increase the decorin expression in ChP and decrease the decorin expression in the PV positive interneurons of hippocampus. As ChP is the main source of CSF production where from CSF is transported through the ventricles and interact with the glymphatic system in the perivascular space and pulsed through the brain parenchyma in the form of interstitial fluid, these changes separately or together may explain the increase of decorin in CSF in the $App^{NL\text{-}F/NL\text{-}F}$ mice.

Decorin activates autophagy in endothelial cells, through VEGFR2/AMPKα activation and mTOR inhibition (*49*), and in breast carcinoma cells (*49-53*) and activates autophagy flux in glioma cells (*55*) and intestinal cells (*56*). We now extend this to include also neuronal autophagy, where autophagy-lysosomal degradation is activated *in vitro* by decorin, mainly targeting the lysosomal function. In endothelial cells paternally expressed gene 3 (Peg3), an imprinted tumor-suppressor gene (*56, 57*), plays a critical role in decorin induced autophagy activation (*49, 52*). Interestingly, we find a substantial amount of accumulated p62 in the tunica intima of AD brains in late stage of the disease progression which may indicate autophagy-inhibition in this part of the vasculature including the endothelial cells. Furthermore, Peg3 is necessary for the transcriptional induction of the Beclin 1 and LC3 (*39, 53*). Therefore, the potential involvement of Peg3 in neuronal autophagy regulation needs to be addressed as well as receptors involved in the binding of decorin and their downstream signaling pathways. Increased knowledge on decorin could further shed light on the possibility of targeting and restoring autophagy in ameliorating AD pathologies. Indeed, preclinical studies using rapamycin to activate autophagy increases

the clearance of Aβ and improves the cognition in AD mouse models (*58, 59*) indicating a therapeutic window for autophagy in AD.

In summary, CSF-decorin level is found to be increased both in AD mice during early Aβ amyloidosis, which correlates with both the decorin expression and Aβ pathology in the brain, and in CSF from preclinical a+t- AD subjects, where it strongly correlates with CSF-amyloid, CSF-t-tau and CSF-p-tau. Therefore, decorin, as an ECM protein as well as autophagy associated protein, can be a potential CSF biomarker of early Aβ amyloidosis.

Methods

Human brain samples

Human brain slides were provided by the brain bank of Karolinska Institutet (approval nr 2013/1301-31/2) (**Supplementary Table 7**).

Animals

App^{NL-F} and App^{NL-G-F} knock-in mice have been described previously (*10*). App^{NL-F} mice contain the Swedish (KM670/671NL) and the Beyreuther/Iberian (I716F) mutations whereas App^{NL-G-F} mice have additionally the Arctic (E693G) mutation inserted into the mouse *App* gene (*10*). Animal experiments were performed under ethical permit ID 407 approved by Linköping animal ethical board. Mice were kept on 12:12 light-dark cycle and with *ad libitum* access to food.

Mouse CSF collection and brain dissection

The mice were anesthetized by isoflurane and placed on the heating pad with fixed heads (the head angle was around 135° from the body) on the stereotaxic instrument. The skin was incised sagittally after removal of the fur. Under the dissection microscope, subcutaneous tissues and muscles were separated to expose the dura mater of cisterna magna. In order to remove the blood contamination, the exposed dura mater was cleaned by PBS-soaked cotton swabs and punctured with a 27-gauge needle avoiding blood vessels. CSF was sampled with a glass capillary and collected in low affinity Eppendorf tubes and directly frozen. The collected CSF was discarded if there was any blood contamination under microscope inspection. Thereafter, the mice were perfused with PBS through cardiac perfusion, and hippocampus and cortex were dissected.

Primary neuron culture

Twenty-four well plates were coated with Poly-D-lysine (Sigma, cat. P6407) for 1 hour at room temperature and washed with Milli-Q water followed by drying overnight. Embryos were separated from $App^{wt/wt}$ mice E16-E18 and the heads were kept in HBSS (ThermoFisher, Cat. 14175095) on ice for brain dissections. Brains were dissected under the dissection microscope to separate the cortex/hippocampus. Cortex/hippocampus were chopped and transferred to the falcon tube together with HBSS. HBSS was

removed until only tissues were left at the bottom. Neurobasal medium (ThermoFisher, Cat. 21103049) 97% + B-27 (ThermoFisher, Cat. 17504044) 2% + Glutamax (ThermoFisher, Cat. 35050038) 1% were added to the tissues and tissues were separated by pipetting up and down 20-30 times. Cells were counted by a hematocytometer with trypan blue staining. 1.5×10^5 cells were seeded in coated 24 well plates. After one week, 50% of the medium was replaced by a fresh medium. After 18 DIV, cells were treated with 200 nM recombinant mouse decorin (R&D, Cat. 1060-DE-100) and/or 100 nM bafilomycin A1 (Sigma, Cat. B1793) for 6 hours then the cells were collected in PBS. Cell solutions were centrifuged at 1,500 rpm for 5 min at 4 °C to pellet the cells, which were lysed in RIPA buffer (ThermoFisher, Cat. 89901). The lysate was sonicated for 1 min and centrifuged at 15,000 rpm for 20 min at 4 °C. The supernatant was transferred to new tubes for western blot. Protein concentration was measured by BCA Protein Assay Kit (ThermoFisher, Cat. 23225). SDS sample buffer containing 0.1 M dithiothreitol was loaded to the samples for western blot analysis.

Immunohistochemistry

For human brain samples, DAB staining was performed with Dako EnVision Systems/HRP (Agilent Technologies, Cat. K401011-2). Slides were deparaffinized by xylene and ethanol and blocked by peroxidase (Dako kit) for 5 min and blocked with 10% normal goat serum for 20 min at room temperature. The slides were incubated with anti-p62 antibody (Cell signaling, Cat. 5114) or anti-Atg5 antibody (R&D, Cat. NB110-53818) in 3% normal goat serum for overnight. After washing with 0.05% PBS-T buffer, slides were incubated with an anti-rabbit secondary antibody (Dako kit) for 30 min at room temperature, followed by incubating with chromogen solution, which was diluted in DAB substrate buffer (Dako kit), for 5 min at room temperature. Before mounting, slides were counterstained with Mayer's Hematoxylin for 30 sec and processed by dehydration. Images were acquired by the Nikon light microscope and were quantified by ImageJ software.

For mouse brain samples, paraffin-embedded brains were sectioned into 4 μm thick sections for most of immunofluorescence staining except vessel staining used 10 μm thick sections. For decorin staining, slides were treated with 0.5 units of chondroitinase ABC (Sigma, Cat. C2905-10UN) in 0.1 M Tris-acetate (PH7.3) for 4 hours in 37 °C before blocking (*47*). For other antibodies, antigen retrieval was performed, whereas the combination of autoclave and chondroitinase ABC treatment was performed for double staining. After blocking, slides were incubated with anti-Aβ antibody (82E1) (Immuno-Biological Laboratories, cat.10323) (1: 2000), anti-decorin antibody (Thermofisher, Cat. PA513538) (single staining 1: 500, double staining 1: 50), anti-decorin antibody (R&D Systems, Cat. AF1060) (1: 200), anti-αSMA antibody (Sigma, Cat. F3777) (1: 500), anti-parvalbumin antibody (Sigma, Cat. MAB1572) (1: 4000) and anti-somatostatin antibody (Sigma, Cat. MAB354) (1: 100), p62 (1: 100) for overnight at 4°C respectively. The following day, slides were incubated with secondary antibodies: Biotinylated goat anti-Rabbit IgG (BioNordika, Cat. BA-1000) (1: 200), Biotinylated goat anti-mouse IgG (BioNordika, Cat. BA-9200) (1: 200), Biotinylated goat anti-rat IgG (BioNordika, Cat. BA-9400) (1: 200), Alexa 546 goat anti-rabbit (Invitrogen, Cat. A11035) (1: 1000), Alexa 555 Donkey anti-goat (Invitrogen, Cat. A21432) (1: 1000). The biotinylated secondary antibodies were amplified with TSA Fluorescein System (PerkinElmer, Cat. NEL701001KT).

Images were acquired by the Nikon Eclipse E800 microscope with Nikon DS-Qi2 camera and were quantified by ImageJ software.

Western Blot

Fresh frozen mouse brain samples were homogenized and separated into cytosolic and membrane fractions. Tissues were homogenized in 10 mM Tris (PH: 8.0) and 0.25 M sucrose and centrifuged at 4,000 rpm for 15 min at 4 °C. Supernatant was centrifuged at 53,000 rpm for 1 h at 4 °C. The supernatant was kept as a cytosolic fraction. Samples were boiled at 95 °C for 3 min. 20 µg proteins were loaded onto 4-20% SDS-PAGE for separation and transferred to PVDF membranes. The PVDF membranes were blocked by 5% skim milk and were probed by primary antibodies, p62 (1: 500), anti-LC3 (Novus Biologicals, Cat. NB100-2331) (1: 1000), anti-β-actin (Sigma, Cat. A2228) (1: 10000) overnight at 4°C. The next day, the PVDF membranes were incubated with fluorescently labeled secondary antibodies (Li-Cor), Donkey anti-rabbit (Cat. 926-32213) (1: 10000) or Goat anti-mouse (Cat. 926-68070) (1: 10000) for 1 hour at room temperature. Images were acquired by a fluorescence imaging system (Li-Cor, Odyssey CLx) and were analyzed by Image Studio Lite (Li-Cor) software.

RNA extraction, cDNA synthesis and qPCR

Fresh mouse brain tissue was kept in RNAprotect Tissue Reagent (Qiagen, Cat. 76104) and RNA was extracted according to the manufacturer's instruction of RNeasy Lipid Tissue Mini Kit (Qiagen, Cat. 74804). After measuring RNA concentration, 200 ng of RNA was used for cDNA synthesis according to manufacturer's instructions of the High-Capacity cDNA Reverse Transcription Kit (Thermofisher, Cat. 4374966). The TaqMan Fast Advanced Master Mix (Thermofisher, Cat. 4444557) was used to perform the qPCR using TaqMan mouse gene expression assays (FAM) (Thermofisher, Cat. 4331182), Mm00448091_m1 for Sqstm1 (Gene aliases: p62). The gene expression level was normalized to TaqMan mouse gene expression assays (VIC) (Thermofisher, Cat. 4448489), Mm02619580_g1 for Atcb. Each sample was triplicated and run in the 7500 Fast Real-Time PCR System (Applied Biosystems).

Mass spectrometry analysis of mouse CSF

An aliquot of 8 µL of each CSF sample was used for in-solution digestion. Briefly, the proteins were re-dissolved in 50 µL of digestion buffer (6 M urea, 100 mM TEAB). A volume of 10 µL of 45 mM aqueous dithiothreitol was added to all samples and the mixtures were incubated at 50°C for 15 min to reduce cysteine disulfides. The samples were cooled to room temperature and 10 µL of 100 mM aqueous iodoacetamide was added before incubating the mixtures for an additional 15 min at room temperature in darkness to carbamidomethylate the cysteines. Finally, 10 µL of 0.1 µg/µL trypsin/Lys-C mixture dissolved in 50 mM ammonium bicarbonate was added to the samples. The tryptic digestion was performed at 37°C overnight. Prior to MS analysis, the peptides were purified and desalted using SPE Pierce C18 Spin Columns (Thermo Scientific). The columns were activated by 2 × 200 µL of 50% acetonitrile and equilibrated with 2 × 200 µL of 0.5% trifluoroacetic acid. The tryptic peptides were adsorbed to the media using two repeated cycles of 40 µL sample loading and the column was washed

using 3 × 200 µL of 0.5% trifluoroacetic acid. Finally, the peptides were eluted in 3 × 50 µL of 70% acetonitrile and dried. Dried peptides were resolved in 21 µL of 0.1% formic acid prior to nano-LC-MS/MS. The nano-LC-MS/MS experiments were performed using a Q Exactive Orbitrap mass spectrometer (ThermoFisher Scientific, Bremen, Germany) equipped with a nano electrospray ion source. The peptides were separated by C18 reversed phase liquid chromatography using an EASY-nLC 1000 system (Thermo Fisher Scientific). A set-up of pre-column and analytical column was used. The precolumn was a 2 cm PepMap Acclaim (C18 100 µm, 5 µm particles) (Thermo Fisher Scientific) while the analytical column was a 10 cm EASY-Spray column (C18 75 µm, 3 µm particles, Thermo Fisher Scientific). Peptides were eluted with a 150 min linear gradient from 4% to 100% acetonitrile at 250 nL min-1. The mass spectrometer was operated in positive ion mode, acquiring a survey mass spectrum with resolving power 70,000 (full width half maximum), m/z 400-1750 using an automatic gain control target of 3×10^6. The 10 most intense ions were selected for higher-energy collisional dissociation fragmentation (25% normalized collision energy) and MS/MS spectra were generated with an automatic gain control target of 5×10^5 at a resolution of 17,500. The mass spectrometer was operated in data-dependent mode. Acquired raw files were processed by MaxQuant (version 1.5.1.2) (the software is available at http://www.maxquant.org). Tandem mass spectra were searched with Andromeda against the UniProt Mus musculus database (release January 2017). The search settings were set as: maximum 10 ppm and 0.02 Da error tolerance for the survey scan and MS/MS analysis respectively; enzyme specificity was trypsin/Lys-C; maximum two missed cleavage sites were allowed; cysteine carbamidomethylation was set as static modification, and Oxidation (M) was set as dynamic modification.

The search criteria for protein identification were set to at least two matching peptides. No proteins were identified and quantified using only one peptide. A maximum false discovery rate of 1% for peptides and proteins was selected. Both razor and unique peptides were used for quantification. A decoy sequence database was built by reversing the target sequence database. A list of known contamination was also included in the identification. The protein intensity values were used for further data analysis.

Mass spectrometry analysis of human CSF

CSF proteomic results reported in a previous study were included in the present research (*33*). Briefly, we selected individuals with AD pathology defined as abnormal CSF Aβ42, and we subdivided this group into abnormal (a+t+, n = 151) and normal CSF t-tau groups (a+t-, n = 77). Based on their cognitive performance, AD individuals were classified in 3 clinical stages as preclinical AD (normal cognition, *i.e.*, NC), prodromal AD (mild cognitive impairment, *i.e.*, MCI) and mild to moderate AD-type dementia according to study specific criteria (*34*). MS was performed using tandem mass tag technique with 10+1 plexing as previously described, using high-pH reverse phase HPLC for peptide prefractionation (*33, 61*). The EMIF-AD MS proteomics data have been deposited to the ProteomeXchange Consortium via the PRIDE partner repository with the dataset identifier 10.6019/PXD019910 (*61*). Fold changes were computed for a+t- and a+t+ groups according to a control group (n = 82) with intact cognition and normal CSF amyloid and tau markers.

Proximity extension assay

One µL of mouse CSF samples were applied to Mouse Exploratory Panel, Olink according to manufacturer's protocol.

Comparison of mouse and human CSF proteomes and analysis of biological processes

The same protein identifiers were used to compare mouse and human CSF proteomes. We performed two types of comparisons. In the first exploratory comparison, proteins with fold change > 1.0 was considered to be upregulated whereas <1.0 was considered downregulated in the mouse and human CSF proteomes. In the second comparison only signifcantly changed proteins in the mouse and human CSF samples ($p < 0.05$) were compared. The proteins in the mouse CSF proteomes that were similarly changed as compared to the human CSF proteomes were further separated depending on whether they were commonly or specifically changed in the two $App^{NL\text{-}F/NL\text{-}F}$ and $App^{NL\text{-}G\text{-}F/NL\text{-}G\text{-}F}$ mouse models respectively, and visualized by Venn diagrams. Commonly up- and down-regulated proteins in both *App* knock-in mouse models and similarly altered in all three stages NC, MCI and AD of the human cohorts were further subjected to gene ontology enrichment analysis (*62-64*). The biological processes with false discovery rate < 0.05 were considered as significantly enriched.

Statistical analysis

For the analysis of mouse CSF proteomics data, protein intensities were first transformed to log2 scale and a two-tailed Student's t-test was performed on proteins which were identifed in all samples in order to identify proteins that were significantly altered in *App* knock-in mouse models, using Qlucore software. A $p < 0.05$ was considered as statistically significant. Venn diagrams were generated by the Interactive Venn tool (*66*) or Venny 2.1 (*67*). To investigate the variation among individual mouse CSF proteomes, a principal component analysis (PCA) was performed in Qlucore. Volcano plots were generated by GraphPad Prism 8 and significantly altered proteins in *App* knock-in models, $p < 0.05$, were indicated. In order to visualize the significantly altered proteins in *App* knock-in mice, heat maps were generated by Morpheus software from the Broad Institute [Morpheus, https://software.broadinstitute.org/morpheus]. For the analysis of biochemical data, one-way ANOVA followed by Dunnett's multiple comparisons test was performed for the three group comparisons while student's t-test was performed for the two-group comparisons in GraphPad Prism 8 when the datasets were normally distrubuted. If the dataset was not noramlly distributed, non-parametric Kruskal-Wallis tests with Dunn's post hoc analysis was used.

Assocations between human CSF-decorin levels (outcome) and CSF amyloid, t-tau and p-tau levels (predictors) were determined using linear regression across the total group, and differences between subgroups (*i.e.*, a-t-, a+t-) in NC group were tested with the 'emtrends' function from the emmeans R package (v1.5.2).

The correlation analysis between parameters of Aβ pathology, autophagy status and decorin expression in the mice were made by Spearman's rank correlation coefficient since some of the parameters were not

normally distributed. The data were grouped from $App^{wt/wt}$ and $App^{NL-F/NL-F}$ mice and $App^{wt/wt}$ and $App^{NL-G-F/NL-G-F}$ mice, respectively.

Data availability

The EMIF-AD mass spectrometry proteomics data have been deposited to the ProteomeXchange Consortium via the PRIDE partner repository with the dataset identifier 10.6019/PXD019910.

Declarations

Acknowledgements

We thank Takashi Saito and Takaomi Saido at RIKEN Center for Brain Science for providing *App* knock-in mice.

Funding: We thank the following financial support; Hållsten Research Foundation (PN), Swedish Research Council (PN), Swedish Brain foundation (PN), Torsten Söderberg Foundation (PN), Sonja Leikrans donation (PN), The Erling-Persson Family Foundation (PN) and China Scholarship Council (RJ). Swedish Research Council 2015-4870 (JB). European Union's Horizon 2020 research and innovation program under the Marie Sk1odowska-Curie grant agreement number 676144 (Synaptic Dysfunction in Alzheimer Disease, SyDAD) (US, VJ, HH), Gun and Bertil Stohne's Research Scholarship (US, HH), Gamla Tjänarinnor grant (US, VJ, PN, JG), Swedish Research Council 2015-4870 (JB), Margaretha af Ugglas Stiftelse (BW). HZ is a Wallenberg Scholar supported by grants from the Swedish Research Council (#2018-02532), the European Research Council (#681712), Swedish State Support for Clinical Research (#ALFGBG-720931), the Alzheimer Drug Discovery Foundation (ADDF), USA (#201809-2016862), and the UK Dementia Research Institute at UCL. JG is supported by Alzheimerfonden (#AF-930934).

Author contributions

RJ and PN initiated the project and designed the study. Most of biochemical experiments were conducted by RJ and part of mouse immunohistochemistry was done by RMH. Mouse CSF collection was done by US; label free mass spectrometry was conducted by GS, JB; the data was analyzed by GS, JB, US, RJ, PN. The mass spectrometry data of human CSF was provided by BMT, PJV, HZ, JG. The comparison of mouse and human CSF mass spectrometry data was analyzed by HH, RJ. The correlation analysis was conducted by AA, RJ. The first draft of manuscript was written by RJ, PN and BW, VJ and SF gave advice to the study and commented on the manuscript. All the authors reviewed and revised the paper.

Competing interests

HZ has served at scientific advisory boards for Denali, Roche Diagnostics, Wave, Samumed, Siemens Healthineers, Pinteon Therapeutics and CogRx, has given lectures in symposia sponsored by Fujirebio, Alzecure and Biogen, and is a co-founder of Brain Biomarker Solutions in Gothenburg AB (BBS), which is

a part of the GU Ventures Incubator Program (outside submitted work). The other authors declare no conflict of interest.

References

1. 1. s. D. International. (Alzheimer's Disease Internationals London, 2019).
2. J. B. Toledo, S. E. Arnold, K. Raible, J. Brettschneider, S. X. Xie, M. Grossman, S. E. Monsell, W. A. Kukull, J. Q. Trojanowski, Contribution of cerebrovascular disease in autopsy confirmed neurodegenerative disease cases in the National Alzheimer's Coordinating Centre. *Brain* **136**, 2697-2706 (2013).
3. U. Lendahl, P. Nilsson, C. Betsholtz, Emerging links between cerebrovascular and neurodegenerative diseases-a special role for pericytes. *EMBO reports* **20**, e48070 (2019).
4. M. O. Dietrich, C. Spuch, D. Antequera, I. Rodal, J. G. de Yébenes, J. A. Molina, F. Bermejo, E. Carro, Megalin mediates the transport of leptin across the blood-CSF barrier. *Neurobiol. Aging* **29**, 902-912 (2008).
5. L. J. Blair, H. D. Frauen, B. Zhang, B. A. Nordhues, S. Bijan, Y.-C. Lin, F. Zamudio, L. D. Hernandez, J. J. Sabbagh, M.-L. B. Selenica, C. A. Dickey, Tau depletion prevents progressive blood-brain barrier damage in a mouse model of tauopathy. *Acta neuropathologica communications* **3**, 8-8 (2015).
6. P. Ballabh, A. Braun, M. Nedergaard, The blood-brain barrier: an overview: structure, regulation, and clinical implications. *Neurobiol. Dis.* **16**, 1-13 (2004).
7. Z. Cai, P. F. Qiao, C. Q. Wan, M. Cai, N. K. Zhou, Q. Li, Role of Blood-Brain Barrier in Alzheimer's Disease. *J. Alzheimers Dis.* **63**, 1223-1234 (2018).
8. A. D. Theocharis, S. S. Skandalis, C. Gialeli, N. K. Karamanos, Extracellular matrix structure. *Adv Drug Deliv Rev* **97**, 4-27 (2016).
9. F. X. Lepelletier, D. M. Mann, A. C. Robinson, E. Pinteaux, H. Boutin, Early changes in extracellular matrix in Alzheimer's disease. *Neuropathol. Appl. Neurobiol.* **43**, 167-182 (2017).
10. T. Saito, Y. Matsuba, N. Mihira, J. Takano, P. Nilsson, S. Itohara, N. Iwata, T. C. Saido, Single App knock-in mouse models of Alzheimer's disease. *Nat. Neurosci.* **17**, 661-663 (2014).
11. W. H. Yu, A. M. Cuervo, A. Kumar, C. M. Peterhoff, S. D. Schmidt, J.-H. Lee, P. S. Mohan, M. Mercken, M. R. Farmery, L. O. Tjernberg, Y. Jiang, K. Duff, Y. Uchiyama, J. Näslund, P. M. Mathews, A. M. Cataldo, R. A. Nixon, Macroautophagy--a novel Beta-amyloid peptide-generating pathway activated in Alzheimer's disease. *The Journal of cell biology* **171**, 87-98 (2005).
12. P. Nilsson, T. C. Saido, Dual roles for autophagy: Degradation and secretion of Alzheimer's disease Aβ peptide. *Bioessays* **36**, 570-578 (2014).
13. T. Johansen, T. Lamark, Selective autophagy mediated by autophagic adapter proteins. *Autophagy* **7**, 279-296 (2011).
14. S. Pankiv, T. H. Clausen, T. Lamark, A. Brech, J.-A. Bruun, H. Outzen, A. Øvervatn, G. Bjørkøy, T. Johansen, p62/SQSTM1 binds directly to Atg8/LC3 to facilitate degradation of ubiquitinated protein

aggregates by autophagy. *The Journal of biological chemistry* **282**, 24131-24145 (2007).

15. N. Mizushima, T. Yoshimori, Y. Ohsumi, Role of the Apg12 conjugation system in mammalian autophagy. *The international journal of biochemistry & cell biology* **35**, 553-561 (2003).
16. Y. Ichimura, T. Kirisako, T. Takao, Y. Satomi, Y. Shimonishi, N. Ishihara, N. Mizushima, I. Tanida, E. Kominami, M. Ohsumi, T. Noda, Y. Ohsumi, A ubiquitin-like system mediates protein lipidation. *Nature* **408**, 488-492 (2000).
17. J. Hemelaar, V. S. Lelyveld, B. M. Kessler, H. L. Ploegh, A single protease, Apg4B, is specific for the autophagy-related ubiquitin-like proteins GATE-16, MAP1-LC3, GABARAP, and Apg8L. *The Journal of biological chemistry* **278**, 51841-51850 (2003).
18. I. Tanida, T. Ueno, E. Kominami, LC3 conjugation system in mammalian autophagy. *The international journal of biochemistry & cell biology* **36**, 2503-2518 (2004).
19. Y. Kabeya, N. Mizushima, T. Ueno, A. Yamamoto, T. Kirisako, T. Noda, E. Kominami, Y. Ohsumi, T. Yoshimori, LC3, a mammalian homologue of yeast Apg8p, is localized in autophagosome membranes after processing. *The EMBO journal* **19**, 5720-5728 (2000).
20. I. Tanida, T. Ueno, E. Kominami, LC3 and Autophagy. *Methods in molecular biology (Clifton, N.J.)* **445**, 77-88 (2008).
21. B. Boland, A. Kumar, S. Lee, F. M. Platt, J. Wegiel, W. H. Yu, R. A. Nixon, Autophagy induction and autophagosome clearance in neurons: relationship to autophagic pathology in Alzheimer's disease. *J. Neurosci.* **28**, 6926-6937 (2008).
22. W. H. Yu, A. M. Cuervo, A. Kumar, C. M. Peterhoff, S. D. Schmidt, J. H. Lee, P. S. Mohan, M. Mercken, M. R. Farmery, L. O. Tjernberg, Y. Jiang, K. Duff, Y. Uchiyama, J. Nalund, P. M. Mathews, A. M. Cataldo, R. A. Nixon, Macroautophagy - a novel beta-amyloid peptide-generating pathway activated in Alzheimer's disease. *J. Cell Biol.* **171**, 87-98 (2005).
23. R. A. Nixon, J. Wegiel, A. Kumar, W. H. Yu, C. Peterhoff, A. Cataldo, A. M. Cuervo, Extensive involvement of autophagy in Alzheimer disease: An immuno-electron microscopy study. *J. Neuropathol. Exp. Neurol.* **64**, 113-122 (2005).
24. S. Lee, Y. Sato, R. A. Nixon, Lysosomal Proteolysis Inhibition Selectively Disrupts Axonal Transport of Degradative Organelles and Causes an Alzheimer's-Like Axonal Dystrophy. *J. Neurosci.* **31**, 7817-7830 (2011).
25. D. M. Wolfe, J. H. Lee, A. Kumar, S. Lee, S. J. Orenstein, R. A. Nixon, Autophagy failure in Alzheimer's disease and the role of defective lysosomal acidification. *Eur. J. Neurosci.* **37**, 1949-1961 (2013).
26. C. D. Aluise, R. A. Sowell, D. A. Butterfield, Peptides and proteins in plasma and cerebrospinal fluid as biomarkers for the prediction, diagnosis, and monitoring of therapeutic efficacy of Alzheimer's disease. *Biochim. Biophys. Acta* **1782**, 549-558 (2008).
27. K. Blennow, H. Zetterberg, Biomarkers for Alzheimer's disease: current status and prospects for the future. *J. Intern. Med.* **284**, 643-663 (2018).
28. B. Olsson, R. Lautner, U. Andreasson, A. Öhrfelt, E. Portelius, M. Bjerke, M. Hölttä, C. Rosén, C. Olsson, G. Strobel, E. Wu, K. Dakin, M. Petzold, K. Blennow, H. Zetterberg, CSF and blood biomarkers for the

diagnosis of Alzheimer's disease: a systematic review and meta-analysis. *The Lancet. Neurology* **15**, 673-684 (2016).

29. K. E. J. Wesenhagen, C. E. Teunissen, P. J. Visser, B. M. Tijms, Cerebrospinal fluid proteomics and biological heterogeneity in Alzheimer's disease: A literature review. *Crit. Rev. Clin. Lab. Sci.*, 1-13 (2019).
30. M. A. Erickson, W. A. Banks, Age-Associated Changes in the Immune System and Blood–Brain Barrier Functions. *Int. J. Mol. Sci.* **20**, 1632 (2019).
31. A. J. Farrall, J. M. Wardlaw, Blood-brain barrier: ageing and microvascular disease--systematic review and meta-analysis. *Neurobiol. Aging* **30**, 337-352 (2009).
32. A. Montagne, S. R. Barnes, M. D. Sweeney, M. R. Halliday, A. P. Sagare, Z. Zhao, A. W. Toga, R. E. Jacobs, C. Y. Liu, L. Amezcua, M. G. Harrington, H. C. Chui, M. Law, B. V. Zlokovic, Blood-brain barrier breakdown in the aging human hippocampus. *Neuron* **85**, 296-302 (2015).
33. B. M. Tijms, J. Gobom, L. Reus, I. Jansen, S. Hong, V. Dobricic, F. Kilpert, M. ten Kate, F. Barkhof, M. Tsolaki, F. R. J. Verhey, J. Popp, P. Martinez-Lage, R. Vandenberghe, A. Lleó, J. L. Molinuevo, S. Engelborghs, L. Bertram, S. Lovestone, J. Streffer, S. Vos, I. Bos, T. A. s. D. N. Initiative, K. Blennow, P. Scheltens, C. E. Teunissen, H. Zetterberg, P. J. Visser, Pathophysiological subtypes of Alzheimer's disease based on cerebrospinal fluid proteomics. *Brain*, (2020).
34. I. Bos, S. Vos, R. Vandenberghe, P. Scheltens, S. Engelborghs, G. Frisoni, J. L. Molinuevo, A. Wallin, A. Lleó, J. Popp, P. Martinez-Lage, A. Baird, R. Dobson, C. Legido-Quigley, K. Sleegers, C. Van Broeckhoven, L. Bertram, M. Ten Kate, F. Barkhof, H. Zetterberg, S. Lovestone, J. Streffer, P. J. Visser, The EMIF-AD Multimodal Biomarker Discovery study: design, methods and cohort characteristics. *Alzheimers Res. Ther.* **10**, 64 (2018).
35. T. Saito, N. Mihira, Y. Matsuba, H. Sasaguri, S. Hashimoto, S. Narasimhan, B. Zhang, S. Murayama, M. Higuchi, V. M. Y. Lee, J. Q. Trojanowski, T. C. Saido, Humanization of the entire murine Mapt gene provides a murine model of pathological human tau propagation. *J. Biol. Chem.* **294**, 12754-12765 (2019).
36. C. Ma, J. Li, Z. Bao, Q. Ruan, Z. Yu, Serum Levels of ApoA1 and ApoA2 Are Associated with Cognitive Status in Older Men. *Biomed Res Int* **2015**, 481621-481621 (2015).
37. M. Kawano, M. Kawakami, M. Otsuka, H. Yashima, T. Yaginuma, A. Ueki, Marked decrease of plasma apolipoprotein AI and AII in Japanese patients with late-onset non-familial Alzheimer's disease. *Clin. Chim. Acta* **239**, 209-211 (1995).
38. R. Tremblay, S. Lee, B. Rudy, GABAergic Interneurons in the Neocortex: From Cellular Properties to Circuits. *Neuron* **91**, 260-292 (2016).
39. T. Neill, C. Sharpe, R. T. Owens, R. V. Iozzo, Decorin-evoked paternally expressed gene 3 (PEG3) is an upstream regulator of the transcription factor EB (TFEB) in endothelial cell autophagy. *J. Biol. Chem.* **292**, 16211-16220 (2017).
40. R. A. Nixon, The role of autophagy in neurodegenerative disease. *Nat. Med.* **19**, 983-997 (2013).

41. E. Wong, A. M. Cuervo, Autophagy gone awry in neurodegenerative diseases. *Nat. Neurosci.* **13**, 805-811 (2010).
42. Z. Gan-Or, P. A. Dion, G. A. Rouleau, Genetic perspective on the role of the autophagy-lysosome pathway in Parkinson disease. *Autophagy* **11**, 1443-1457 (2015).
43. P. Nilsson, K. Loganathan, M. Sekiguchi, Y. Matsuba, K. Hui, S. Tsubuki, M. Tanaka, N. Iwata, T. Saito, Takaomi C. Saido, Aβ Secretion and Plaque Formation Depend on Autophagy. *Cell Reports* **5**, 61-69 (2013).
44. M. Vanlandewijck, L. He, M. A. Mäe, J. Andrae, K. Ando, F. Del Gaudio, K. Nahar, T. Lebouvier, B. Laviña, L. Gouveia, Y. Sun, E. Raschperger, M. Räsänen, Y. Zarb, N. Mochizuki, A. Keller, U. Lendahl, C. Betsholtz, A molecular atlas of cell types and zonation in the brain vasculature. *Nature* **554**, 475-480 (2018).
45. J. J. Iliff, M. Wang, Y. Liao, B. A. Plogg, W. Peng, G. A. Gundersen, H. Benveniste, G. E. Vates, R. Deane, S. A. Goldman, E. A. Nagelhus, M. Nedergaard, A paravascular pathway facilitates CSF flow through the brain parenchyma and the clearance of interstitial solutes, including amyloid β. *Sci. Transl. Med.* **4**, 147ra111 (2012).
46. U. Lendahl, P. Nilsson, C. Betsholtz, Emerging links between cerebrovascular and neurodegenerative diseases-a special role for pericytes. *EMBO reports* **20**, e48070 (2019).
47. A. D. Snow, H. Mar, D. Nochlin, H. Kresse, T. N. Wight, Peripheral distribution of dermatan sulfate proteoglycans (decorin) in amyloid-containing plaques and their presence in neurofibrillary tangles of Alzheimer's disease. *The journal of histochemistry and cytochemistry : official journal of the Histochemistry Society* **40**, 105-113 (1992).
48. S. Buraschi, T. Neill, R. V. Iozzo, Decorin is a devouring proteoglycan: Remodeling of intracellular catabolism via autophagy and mitophagy. *Matrix Biol.* **75-76**, 260-270 (2019).
49. S. Buraschi, T. Neill, A. Goyal, C. Poluzzi, J. Smythies, R. T. Owens, L. Schaefer, A. Torres, R. V. Iozzo, Decorin causes autophagy in endothelial cells via Peg3. *Proc. Natl. Acad. Sci. U. S. A.* **110**, E2582-E2591 (2013).
50. A. Goyal, T. Neill, R. T. Owens, L. Schaefer, R. V. Iozzo, Decorin activates AMPK, an energy sensor kinase, to induce autophagy in endothelial cells. *Matrix Biol.* **34**, 46-54 (2014).
51. T. Neill, L. Schaefer, R. V. Iozzo, Instructive Rotes of Extracellular Matrix on Autophagy. *Am. J. Pathol.* **184**, 2146-2153 (2014).
52. T. Neill, A. Torres, S. Buraschi, R. V. Iozzo, Decorin has an appetite for endothelial cell autophagy. *Autophagy* **9**, 1626-1628 (2013).
53. T. Neill, A. Torres, S. Buraschi, R. T. Owens, J. B. Hoek, R. Baffa, R. V. Iozzo, Decorin induces mitophagy in breast carcinoma cells via peroxisome proliferator-activated receptor γ coactivator-1α (PGC-1α) and mitostatin. *The Journal of biological chemistry* **289**, 4952-4968 (2014).
54. T. Yao, C. G. Zhang, M. T. Gong, M. Zhang, L. Wang, W. Ding, Decorin-mediated inhibition of the migration of U87MG glioma cells involves activation of autophagy and suppression of TGF-beta signaling. *FEBS open bio* **6**, 707-719 (2016).

55. H. Z. Zhao, H. Q. Xi, B. Wei, A. Z. Cai, T. Wang, Y. Wang, X. D. Zhao, Y. J. Song, L. Chen, Expression of decorin in intestinal tissues of mice with inflammatory bowel disease and its correlation with autophagy. *Exp. Ther. Med.* **12**, 3885-3892 (2016).
56. W. Feng, R. T. Marquez, Z. Lu, J. Liu, K. H. Lu, J. P. Issa, D. M. Fishman, Y. Yu, R. C. Bast, Jr., Imprinted tumor suppressor genes ARHI and PEG3 are the most frequently down-regulated in human ovarian cancers by loss of heterozygosity and promoter methylation. *Cancer* **112**, 1489-1502 (2008).
57. T. Kohda, A. Asai, Y. Kuroiwa, S. Kobayashi, K. Aisaka, G. Nagashima, M. C. Yoshida, Y. Kondo, N. Kagiyama, T. Kirino, T. Kaneko-Ishino, F. Ishino, Tumour suppressor activity of human imprinted gene PEG3 in a glioma cell line. *Genes Cells* **6**, 237-247 (2001).
58. A. Caccamo, S. Majumder, A. Richardson, R. Strong, S. Oddo, Molecular interplay between mammalian target of rapamycin (mTOR), amyloid-beta, and Tau: effects on cognitive impairments. *The Journal of biological chemistry* **285**, 13107-13120 (2010).
59. P. Spilman, N. Podlutskaya, M. J. Hart, J. Debnath, O. Gorostiza, D. Bredesen, A. Richardson, R. Strong, V. Galvan, Inhibition of mTOR by rapamycin abolishes cognitive deficits and reduces amyloid-beta levels in a mouse model of Alzheimer's disease. *PLoS One* **5**, e9979-e9979 (2010).
60. T. S. Batth, C. Francavilla, J. V. Olsen, Off-Line High-pH Reversed-Phase Fractionation for In-Depth Phosphoproteomics. *J. Proteome Res.* **13**, 6176-6186 (2014).
61. Y. Perez-Riverol, A. Csordas, J. Bai, M. Bernal-Llinares, S. Hewapathirana, D. J. Kundu, A. Inuganti, J. Griss, G. Mayer, M. Eisenacher, E. Perez, J. Uszkoreit, J. Pfeuffer, T. Sachsenberg, S. Yilmaz, S. Tiwary, J. Cox, E. Audain, M. Walzer, A. F. Jarnuczak, T. Ternent, A. Brazma, J. A. Vizcaino, The PRIDE database and related tools and resources in 2019: improving support for quantification data. *Nucleic Acids Res* **47**, D442-D450 (2019).
62. M. Ashburner, C. A. Ball, J. A. Blake, D. Botstein, H. Butler, J. M. Cherry, A. P. Davis, K. Dolinski, S. S. Dwight, J. T. Eppig, M. A. Harris, D. P. Hill, L. Issel-Tarver, A. Kasarskis, S. Lewis, J. C. Matese, J. E. Richardson, M. Ringwald, G. M. Rubin, G. Sherlock, Gene ontology: tool for the unification of biology. The Gene Ontology Consortium. *Nat. Genet.* **25**, 25-29 (2000).
63. The Gene Ontology Resource: 20 years and still GOing strong. *Nucleic Acids Res.* **47**, D330-d338 (2019).
64. H. Mi, A. Muruganujan, D. Ebert, X. Huang, P. D. Thomas, PANTHER version 14: more genomes, a new PANTHER GO-slim and improvements in enrichment analysis tools. *Nucleic Acids Res.* **47**, D419-d426 (2019).
65. H. Heberle, G. V. Meirelles, F. R. da Silva, G. P. Telles, R. Minghim, InteractiVenn: a web-based tool for the analysis of sets through Venn diagrams. *BMC Bioinformatics* **16**, 169 (2015).
66. J. C. Oliveros, Venny. An interactive tool for comparing lists with Venn's diagrams., (2007-2015).
67. M. A. Gubbiotti, T. Neill, H. Frey, L. Schaefer, R. V. Iozzo, Decorin is an autophagy-inducible proteoglycan and is required for proper in vivo autophagy. *Matrix Biol.* **48**, 14-25 (2015).
68. X. Li, D. Roife, Y. Kang, B. Dai, M. Pratt, J. B. Fleming, Extracellular lumican augments cytotoxicity of chemotherapy in pancreatic ductal adenocarcinoma cells via autophagy inhibition. *Oncogene* **35**,

4881-4890 (2016).

69. M. Tatti, M. Motta, S. Di Bartolomeo, S. Scarpa, V. Cianfanelli, F. Cecconi, R. Salvioli, Reduced cathepsins B and D cause impaired autophagic degradation that can be almost completely restored by overexpression of these two proteases in Sap C-deficient fibroblasts. *Hum. Mol. Genet.* **21**, 5159-5173 (2012).
70. M. U. Hutchins, D. J. Klionsky, Vacuolar localization of oligomeric alpha-mannosidase requires the cytoplasm to vacuole targeting and autophagy pathway components in Saccharomyces cerevisiae. *The Journal of biological chemistry* **276**, 20491-20498 (2001).
71. Y. S. Hah, H. S. Noh, J. H. Ha, J. S. Ahn, J. R. Hahm, H. Y. Cho, D. R. Kim, Cathepsin D inhibits oxidative stress-induced cell death via activation of autophagy in cancer cells. *Cancer Lett.* **323**, 208-214 (2012).
72. K. L. Chen, W. S. Chang, C. H. Cheung, C. C. Lin, C. C. Huang, Y. N. Yang, C. P. Kuo, C. C. Kuo, Y. H. Chang, K. J. Liu, C. M. Wu, J. Y. Chang, Targeting cathepsin S induces tumor cell autophagy via the EGFR-ERK signaling pathway. *Cancer Lett.* **317**, 89-98 (2012).
73. J. M. Vidal-Donet, J. Cárcel-Trullols, B. Casanova, C. Aguado, E. Knecht, Alterations in ROS activity and lysosomal pH account for distinct patterns of macroautophagy in LINCL and JNCL fibroblasts. *PLoS One* **8**, e55526-e55526 (2013).

Tables

Table 1: Significantly altered autophagy/ECM-associated proteins in mouse CSF identified by MS and PEA.

Autophagy protein	Method	Alterations (log2 fold)	p-value	Autophagy-associated function
Decorin	MS	1.05*	0.003	Decorin can induce autophagy in endothelial cells (*50*). Decorin can be regulated by autophagy (*68*).
		1.05‡	0.013	
Lumican	MS	1.03*	0.01	Lumican inhibits autophagy by decreasing AMPK activity in chemotherapy of pancreatic ductal adenocarcinoma cells (PDACs) (*68*).
		1.04‡	0.002	
Cathepsin B	MS	0.98*	0.017	Reduced cathepsins B and D cause impaired autophagic degradation (*69*).
		1.02#	0.026	
		0.97‡	0.002	
Alpha-mannosidase (Ams1)	MS	0.98*	0.045	Ams1 is delivered to vacuoles by cytoplasm to vacuole targeting (Cvt) pathway and autophagy pathway (*71*).
Cathepsin D	MS	0.98‡	0.017	High level of Cathepsin D significantly activates autophagy in HeLa cells (*71*).
Cathepsin S	MS	0.98‡	0.009	Cathepsin S is a member of lysosomal cysteine cathepsin family and play a key role in autophagy regulation (*72*).
Tripeptidyl-peptidase 1 (Tpp1)	PEA	1.3#	0.002	Loss of Tpp1 function decreases the autophagic degradation (*73*).

ECM protein	Method	Alterations (log2 fold)	p-value
Decorin	MS	1.05*	0.003
		1.05‡	0.013
Lumican	MS	1.03*	0.01
		1.04‡	0.002
Collagen alpha-1(I) chain	MS	0.95#	0.004
		1.06‡	0.002
Basement membrane-specific heparan sulfate proteoglycan core protein	MS	0.97#	0.01
Fibronectin	MS	0.98*	0.049
		0.97#	0.038
SPARC-like 1	MS	0.97*	0.022
		0.97#	0.04
Fibulin-1	MS	0.96#	0.041
Vitronectin	MS	0.97#	0.042
Ecm1 protein	MS	0.97#	0.045
Procollagen C-endopeptidase enhancer protein	MS	1.02‡	0.033
CCN family member 4	PEA	1.51‡	0.004
Matrilin-2	PEA	0.93*	0.016
		0.87#	0.008

*$App^{NL\text{-}F/NL\text{-}F}$ vs $App^{wt/wt}$; #$App^{NL\text{-}G\text{-}F/NL\text{-}G\text{-}F}$ vs $App^{wt/wt}$; ‡$App^{NL\text{-}F/NL\text{-}F}$ vs $App^{NL\text{-}G\text{-}F/NL\text{-}G\text{-}F}$

Figures

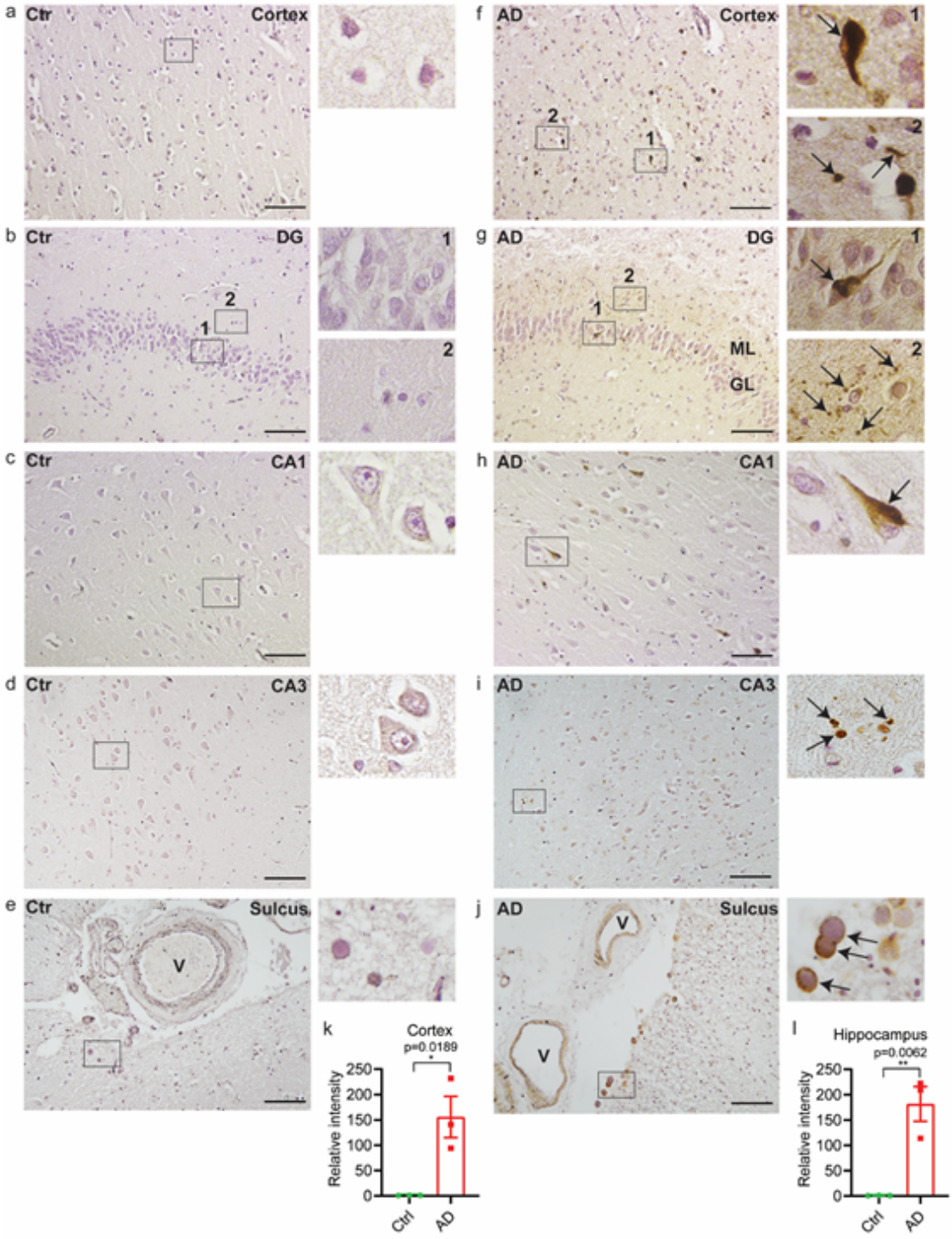

Figure 1

p62 accumulates in AD brains. Immunohistochemistry of p62 in entorhinal cortex (a, f), different regions of hippocampus DG (b, g), CA1 (c, h), CA3 (d, i) and sulcus (e, j) from healthy control (Ctr) and AD brains. Higher magnification images of depicted areas (black boxes) are shown to the right. Arrows in (f) 1, (g) 1 and (h) indicates p62 accumulation in neurons of entorhinal cortex and hippocampus; (f) 2 indicates small round dots or outstretched shape of p62 accumulations; (g) 2 indicates potential axonal beadings

in ML of DG; (i) indicates potential apoptotic bodies; (j) indicates corpora amylacea. p62 is accumulated in tunica intima of the vessels in AD (j). V: vessel; ML: molecular layer; GL: granular layer. Semi-quantitative density measurement was performed for quantification. 20x magnification images of three different regions (without overlapping) of cortex were chosen from each individual and the intensities were quantified (k). 20x magnification images of DG, CA1, CA3 (one for each region) were chosen for hippocampus and the intensities were quantified (l). Scale bars represent 100 μm. (n = 3, *p < 0.05, **p < 0.01). Data are represented as mean ± SEM.

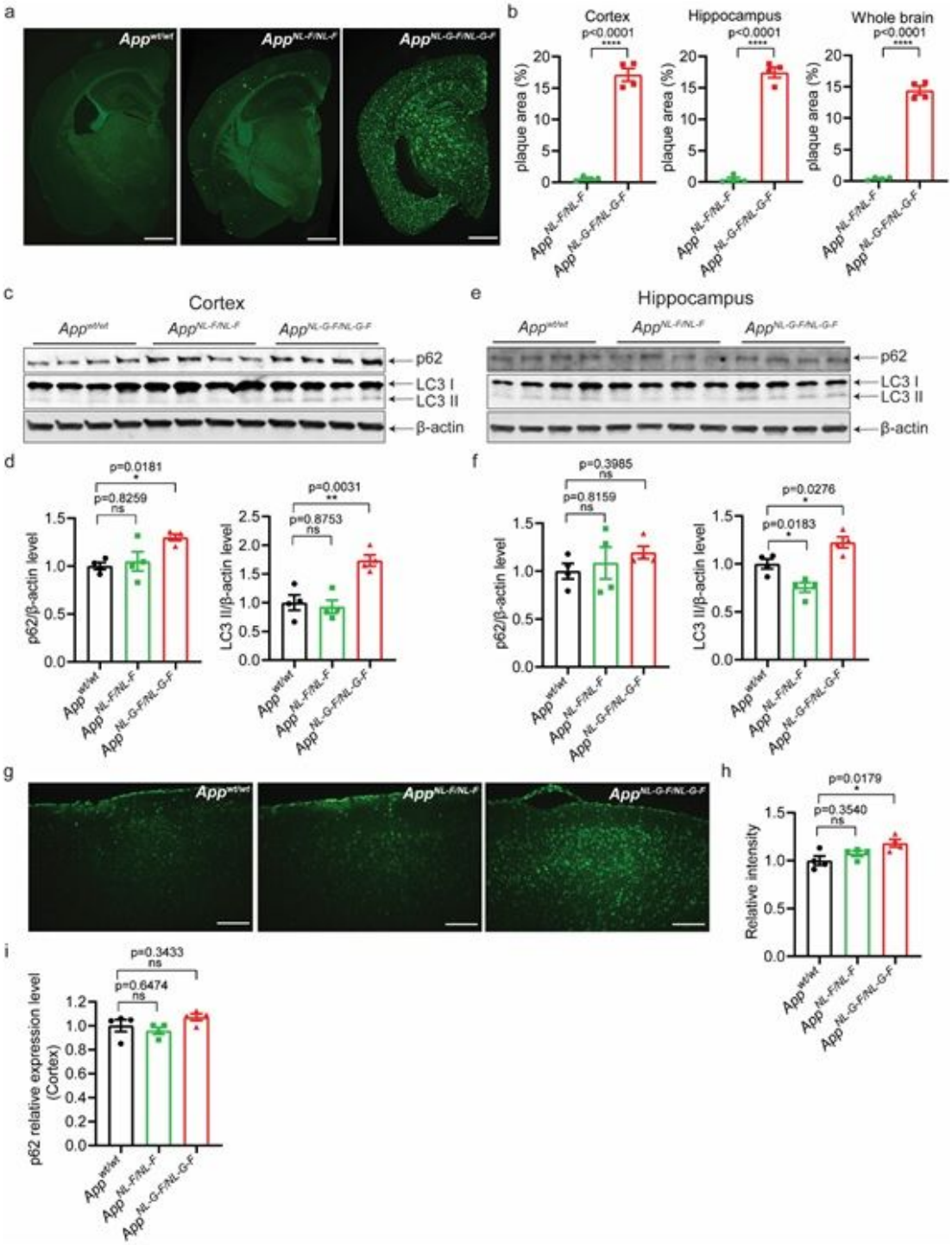

Figure 2

Autophagy is impaired in AppNL-G-F/NL-G-F mice. (a) Immunostaining of Aβ in 12-month-old Appwt/wt, AppNL-F/NL-F and AppNL-G-F/NL-G-F mouse brains show Aβ deposition. Scale bars represent 1000 μm. (b) The quantification of the percentage of plaque areas in cortex, hippocampus and whole brain of AppNL-F/NL-F and AppNL-G-F/NL-G-F mice. The Appwt/wt mice were not included in the quantification analysis because of the lack of human Aβ plaque deposition. (n = 4, ****p < 0.0001). Cytosolic fraction of cortical (c) and hippocampal (e) brain homogenates from 12-month-old Appwt/wt, AppNL-F/NL-F and AppNL-G-F/NL-G-F mice were immunoblotted with autophagic markers p62 and LC3. The levels of p62 and LC3 II in cortex (d) and hippocampus (f) were quantified by densitometry. (n = 4, *p < 0.05, **p < 0.01). (g) Immunostaining of p62 in 12-month-old Appwt/wt, AppNL-F/NL-F and AppNL-G-F/NL-G-F mouse cortex. Scale bars represent 100 μm. (h) The intensities were quantified. (n = 4, **p < 0.01). (i) Relative mRNA expression level of p62 in cortex analyzed by qPCR. Data are represented as mean ± SEM.

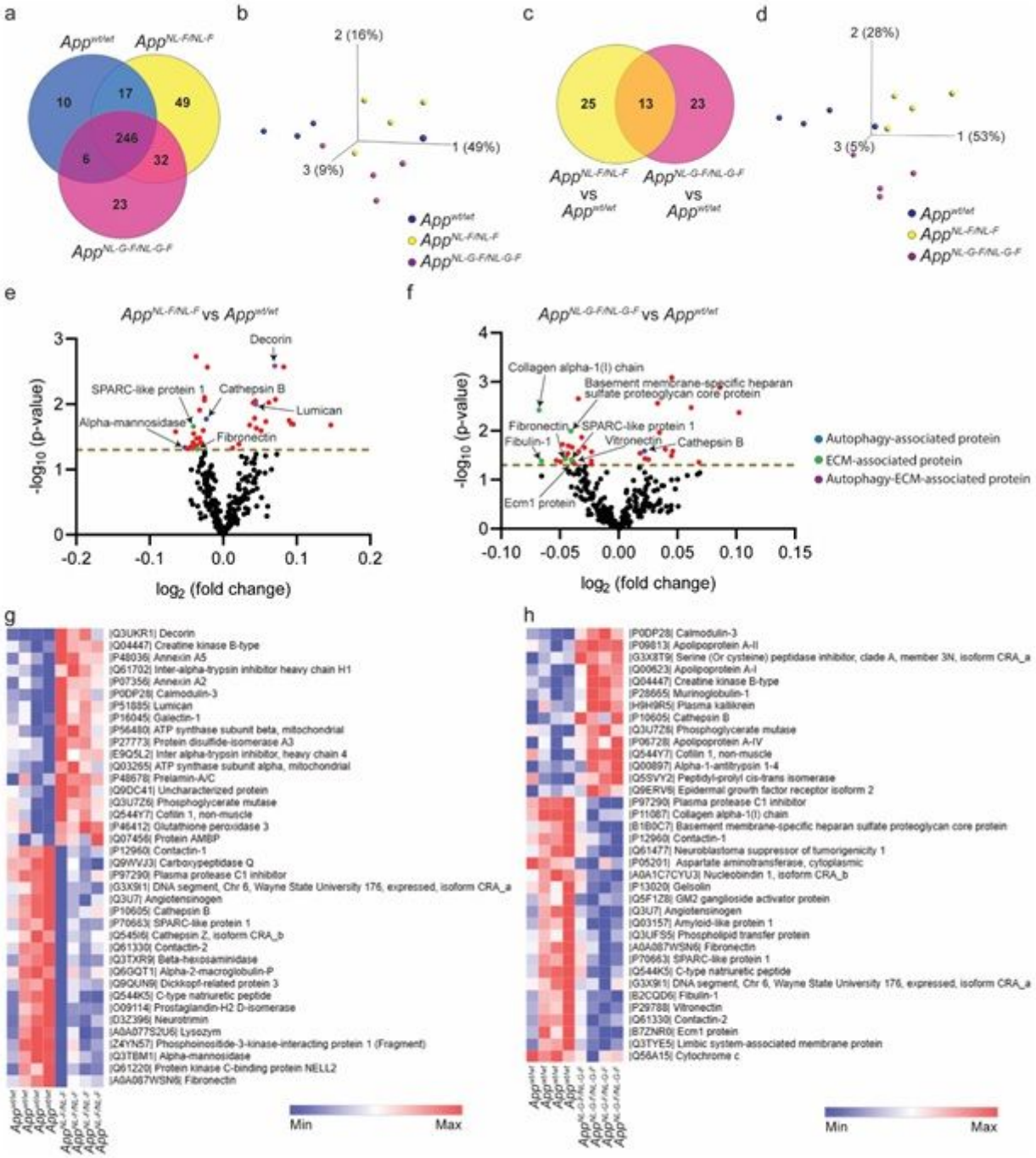

Figure 3

Mass spectrometry analysis of CSF from App knock-in mice identifies changes in autophagy and ECM associated proteins. (a) Venn diagram showing the number of proteins identified in CSF of 12-month-old Appwt/wt, AppNL-F/NL-F and AppNL-G-F/NL-G-F mice. (n = 4) (b) PCA of proteins that were identified in all samples of Appwt/wt and App knock-in mice. (c) Venn diagram showing the number of significantly altered proteins in AppNL-F/NL-F mice and AppNL-G-F/NL-G-F mice as compared to Appwt/wt ($p < 0.05$). (d) PCA of significantly altered proteins in AppNL-F/NL-F mice and AppNL-G-F/NL-G-F mice as compare to Appwt/wt ($p < 0.05$). (e-f) Volcano plots displaying the changes in protein expression in AppNL-F/NL-F

mice and AppNL-G-F/NL-G-F mice, respectively. A cut-off of p-value 0.05 (dash line) was used to highlight the significantly changed proteins. Red dots represent significantly changed proteins; blue dots represent significantly changed autophagy-associated proteins; Green dots represent significantly changed ECM-associated proteins; purple dots represent significantly changed autophagy-ECM-associated proteins; black dots represent not significantly changed proteins. Heatmaps showing the significantly ($p < 0.05$) changed protein names in AppNL-F/NL-F mice (g) and AppNL-G-F/NL-G-F mice (h) as compared to Appwt/wt (red denotes relatively upregulated; blue denotes relatively downregulated).

a

	Abnormal-amyloid/normal-tau						Abnormal-amyloid/abnormal-tau					
	vs $App^{NL-F/NL-F}$			vs $App^{NL-G-F/NL-G-F}$			vs $App^{NL-F/NL-F}$			vs $App^{NL-G-F/NL-G-F}$		
	NC	MCI	AD	NC	MCI	AD	NC	MCI	AD	NC	MCI	AD
Upregulated protein number	33	46	35	38	50	37	39	47	53	38	47	53
Downregulated protein number	76	84	81	84	90	86	24	26	27	26	28	29

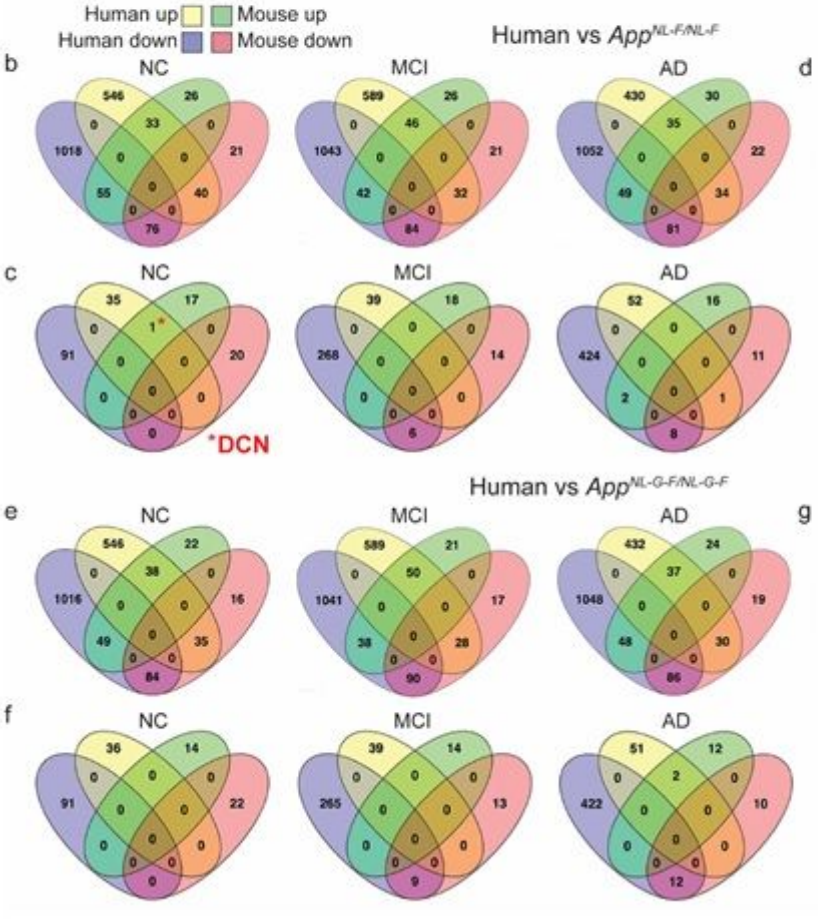

d

NC	MCI	AD
Upregulated	Downregulated	Downregulated
DCN#	DKK3	DKK3
	FAM3C	FAM3C
	NTM	NTM
	PIK3IP1	PIK3IP1
	SPARCL1#	SPARCL1#
	NPPC	NPPC
		FN1#
		CNTN1

g

AD	MCI	AD
Upregulated	Downregulated	Downregulated
APOA1	GM2A	GM2A
APOA2	APLP1	APLP1
	CYCS	CYCS
	FAM3C	FAM3C
	NBL1	NBL1
	SPARCL1#	SPARCL1#
	NPPC	NPPC
	ECM1#	ECM1#
	LSAMP	LSAMP
		GOT1
		FN1#
		CNTN1

Figure 4

Comparison of human and mouse CSF proteomes identifies decorin as significantly increased in NC subjects and AppNL-F/NL-F mice. (a) Number of proteins commonly up or downregulated in App knock-in mice as compared to human cohorts. Venn diagrams showing (b) all upregulated and downregulated proteins and (c) significantly changed proteins ($p < 0.05$) in the CSF of AppNL-F/NL-F mice and

NC/MCI/AD human cohorts from abnormal-amyloid/normal-tau subjects. Among those significantly changed proteins, ECM protein decorin is the only significantly upregulated protein in NC subjects and AppNL-F/NL-F mice. (d) The gene names of significantly upregulated and downregulated proteins in both AppNL-F/NL-F mouse and human CSF. Venn diagrams showing (e) all upregulated and downregulated proteins and (f) significantly changed proteins ($p < 0.05$) in the CSF of AppNL-G-F/NL-G-F mice and NC/MCI/AD human cohorts from abnormal-amyloid/normal-tau subjects. (g) The gene names of significantly upregulated and downregulated proteins in both AppNL-G-F/NL-G-F mouse and human CSF. # denotes ECM-associated proteins.

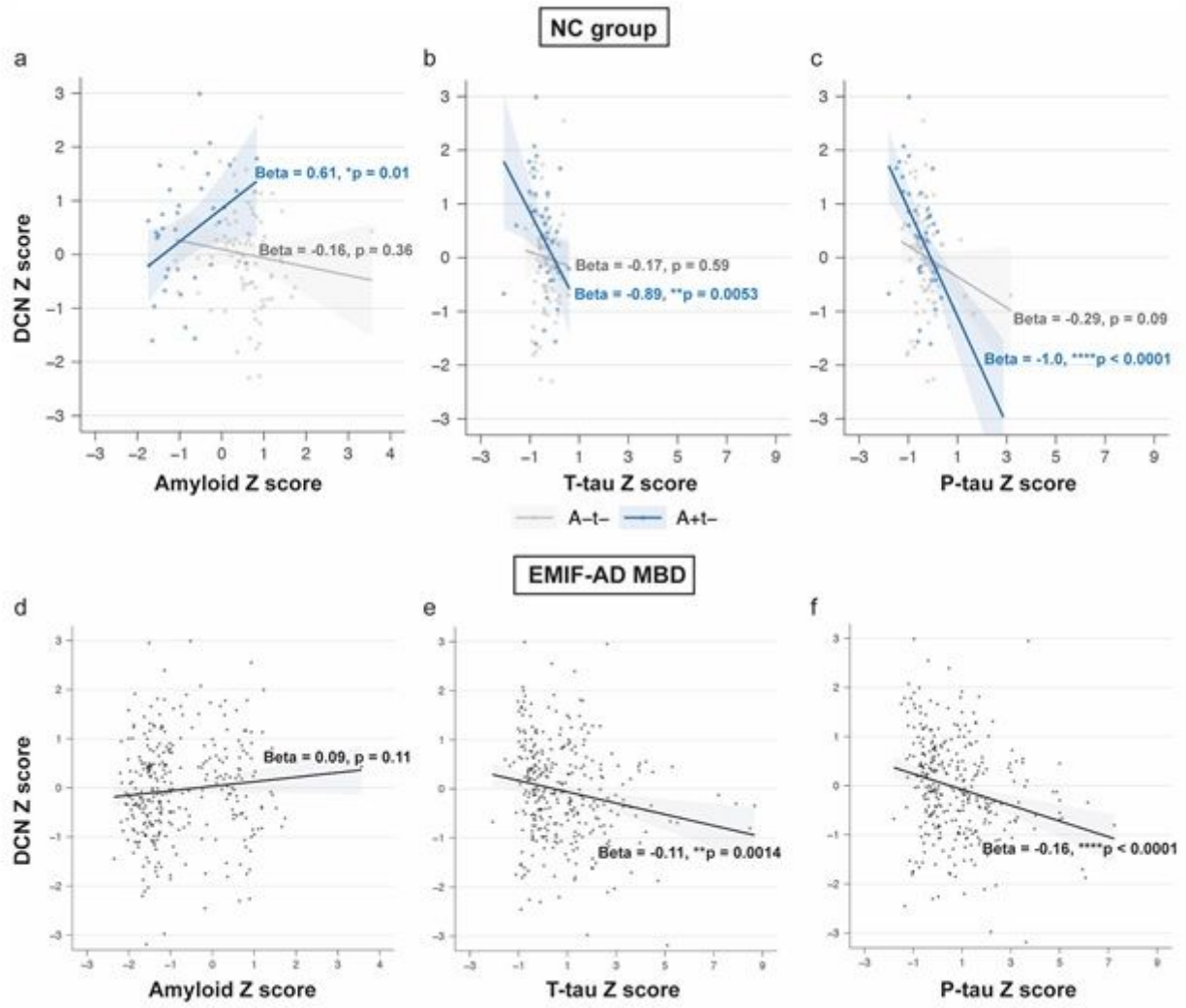

Figure 5

CSF-decorin positively correlates with CSF-amyloid in preclinical AD subjects with abnormal CSF amyloid. In subjects with normal cognition (NC), the correlations of CSF DCN Z score and the Z scores of CSF amyloid (a), CSF t-tau (b), CSF p-tau (c) were analyzed and separated into CSF a-t- (n = 82) and a+t- (n = 36) subjects. In the whole EMIF-AD MBD cohort (n = 310), including NC (n = 139), MCI (n = 92) and AD (n

= 79), the correlations of CSF DCN Z score and the Z scores of CSF amyloid (d), CSF t-tau (e), CSF p-tau (f) were analyzed. The regression coefficients (Beta) and p-values are displayed. DCN: decorin.

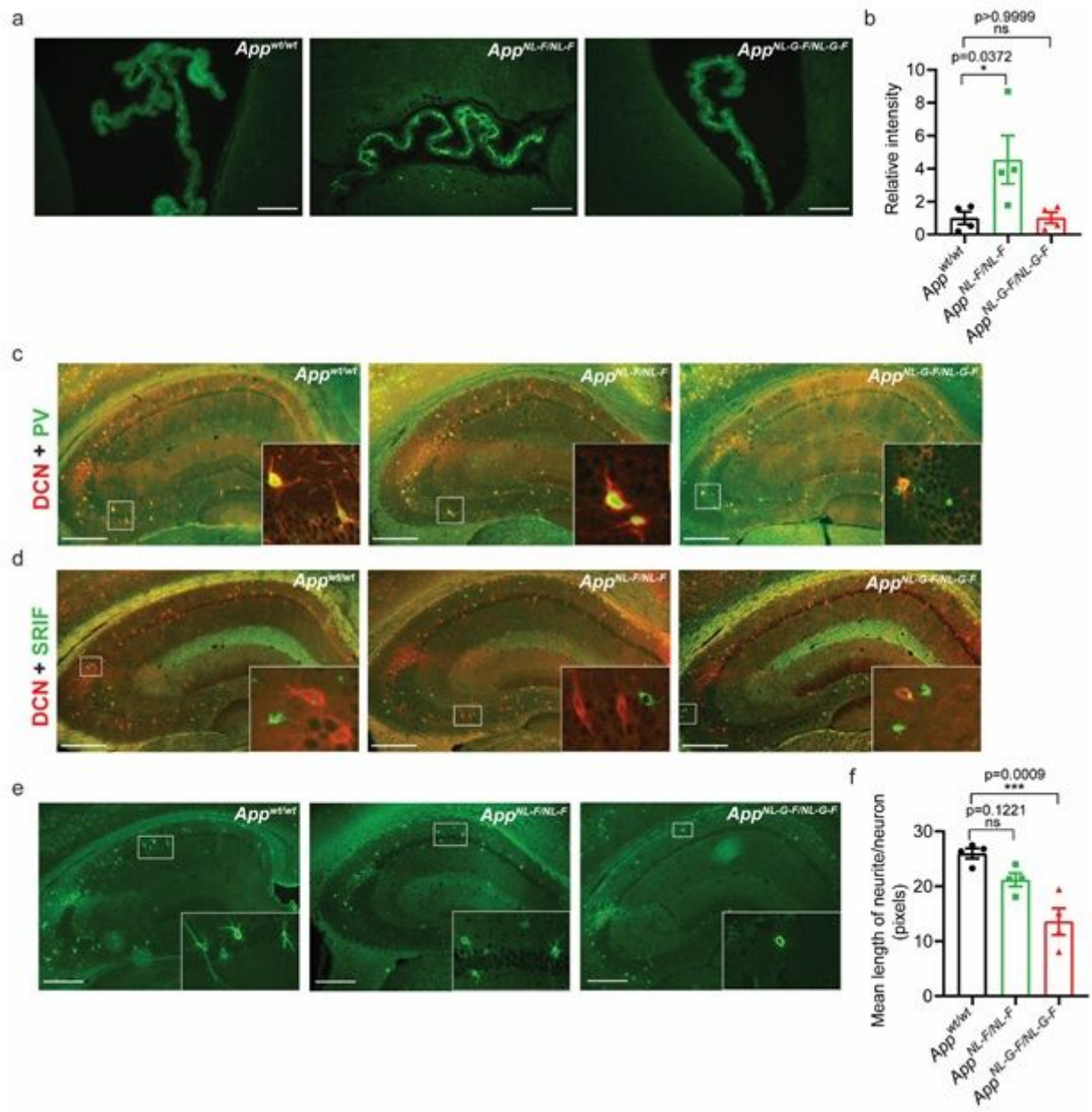

Figure 6

Decorin is increased in choroid plexus (ChP) of AppNL-F/NL-F mice and decreased in interneurons of AppNL-G-F/NL-G-F mice. (a) Immunostaining of decorin in the ChP of 12-month-old Appwt/wt, AppNL-F/NL-F and AppNL-G-F/NL-G-F mice. Scale bars represent 100 μm. (b) The intensities in ChP were quantified. Data was analyzed by Kruskal–Wallis tests followed by Dunn's multiple comparisons test (n = 4, *p < 0.05). (c) Double immunostaining of DCN (red) with PV (green) in mouse hippocampus. Representative decorin positive PV interneurons of Appwt/wt, AppNL-F/NL-F and AppNL-G-F/NL-G-F mice are shown with higher magnification images in the right bottom. Scale bars represent 500 μm. DCN: decorin; PV: parvalbumin. (d) Double immunostaining of DCN (red) with SRIF (green) in mouse

hippocampus. The representative decorin positive and SRIF positive interneurons of Appwt/wt, AppNL-F/NL-F and AppNL-G-F/NL-G-F mice were shown with higher magnification images in the right bottom. Scale bars represent 500 μm. SRIF: somatotropin release-inhibiting factor. (e) The length of neurites from decorin positive PV interneurons were quantified. (n = 4, ***p < 0.001). Data are represented as mean ± SEM.

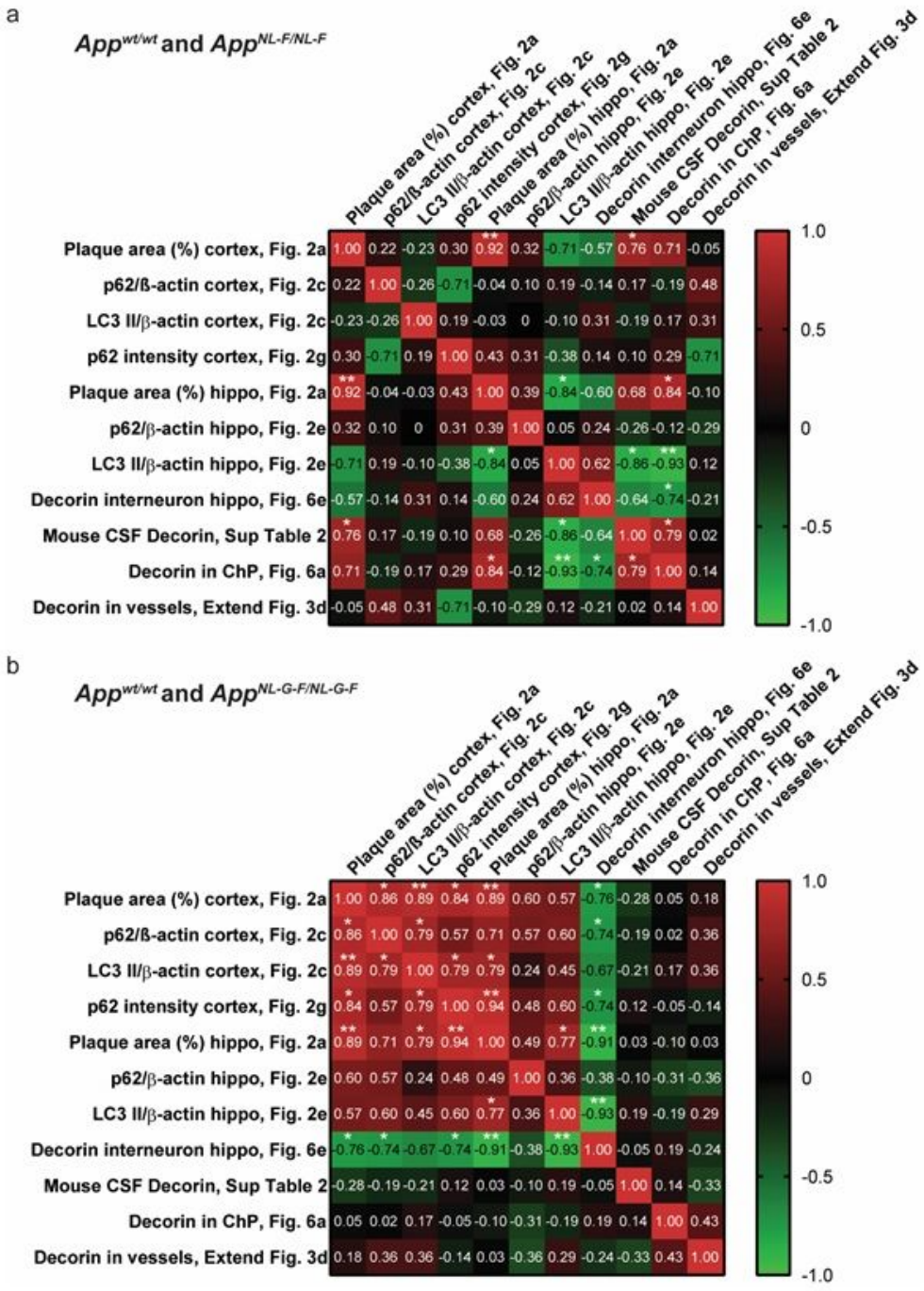

Figure 7

Mouse CSF decorin levels positively correlates with decorin expression in choroid plexus and Aβ amyloidosis in AppNL-F/NL-F mice. Spearman correlation analysis of parameters related to Aβ plaque load, autophagy and decorin expression between AppNL-F/NL-F and Appwt/wt mice (a); AppNL-G-F/NL-G-F and Appwt/wt mice (b) from 12 months old. The corresponding figures for each parameter are denoted. The correlation coefficients are displayed (*p < 0.05, **p < 0.01). The red color represents positive correlation, and the green color represents negative correlation according to the scale bars in the right column.

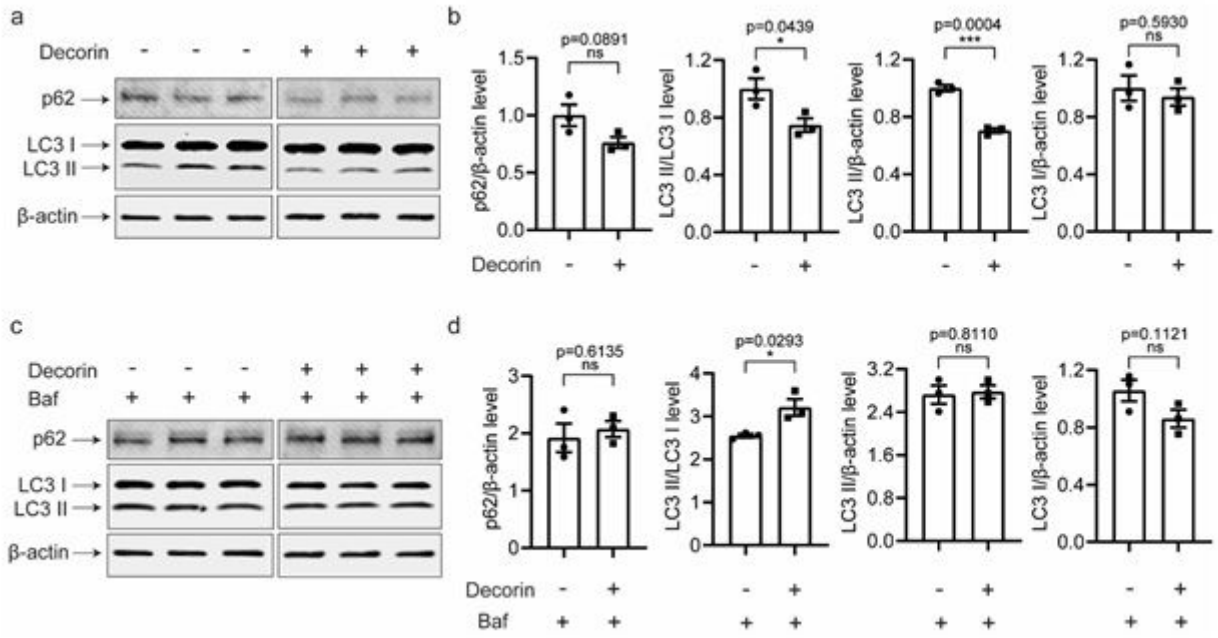

Figure 8

Decorin activates lysosomal degradation involved in autophagy in primary neurons. Western blot analysis of p62 and LC3 in Appwt/wt mouse primary neurons treated with (a) decorin (200 nM) or (c) decorin (200 nM) and Bafilomycin A1 (100 nM) for 6 hours. Each condition is triplicated and the whole set of experiments repeated twice. (b, d) The levels of p62, LC3 I, LC3 II, and LC3 II/LC3 I were quantified by densitometry. (*p < 0.05, ***p < 0.001). Data are represented as mean ± SEM.

Supplementary Files

This is a list of supplementary files associated with this preprint. Click to download.

- SupplementaryTable1.xlsx
- SupplementaryTable2.xlsx
- SupplementaryTable3.xlsx
- SupplementaryTable4.xlsx

- SupplementaryTable5.xlsx
- SupplementaryTable6.xlsx
- SupplementaryTable7.xlsx
- ExtendedFigures.pdf